Dynamics of non-uniform beams for microelectromechanical systems

Sajal Sagar Singh

A Thesis Submitted to

Indian Institute of Technology Hyderabad

In Partial Fulfillment of the Requirements for

The Degree of Master of Technology

Department of Mechanical and Aerospace Engineering

July 2016

Declaration

I declare that this written submission represents my ideas in my own words, and where ideas or words of others have been included, I have adequately cited and referenced the original sources. I also declare that I have adhered to all principles of academic honesty and integrity and have not misrepresented or fabricated or falsified any idea/data/fact/source in my submission. I understand that any violation of the above will be a cause for disciplinary action by the Institute and can also evoke penal action from the sources that have thus not been properly cited, or from whom proper permission has not been taken when needed.

Sajal Sagar Singh

(Signature)

SAJAL SAGAR SINGH

(Sajal Sagar Singh)

mc11b15m000009

(Roll No.)

Approval Sheet

This Thesis entitled Dynamics of non-uniform beams for microelectromechanical systems by Sajal Sagar Singh is approved for the degree of Master of Technology from IIT Hyderabad

(Dr. Jyotsnendu Giri) Examiner
Dept. of Biomed. Eng.
IIT Hyderabad

(Dr. Venkatesham Balide) Examiner
Dept. of Mech. and Aerosp. Eng.
IIT Hyderabad

(Dr. Ashok Kumar Pandey) Adviser
Dept. of Mech. and Aerosp. Eng.
IIT Hyderabad

(Dr. Prem Pal) Co-Adviser
Dept. of Physics
IIT Hyderabad

(Dr. Jyotsnendu Giri) Chairman
Dept. of Biomed. Eng.
IIT Hyderabad

Acknowledgements

When I converted to the Masters program from my Bachelors program at IIT Hyderabad, I was of the notion that the life of a research student is quite rustic. Where else would I get paid for studying what I like! Life was however quite hectic, adventurous and fun-filled than that.

Most of the credit for this work goes to many people whom I have known in the last 5 years at IIT Hyderabad (B.Tech+M.Tech days). To start with my adviser Dr. Ashok Pandey who patiently introduced me to a relatively new feild of vibrations and non-linear dynamics and illuminated me with his amazing understanding and knowledge of the subject. I deeply acknowledge his contribution through enthusiastic discussions, clearing my doubts and helping me with my skwed arguments. His ideology of simplyfying the problems of science is something which has improved my way of thinking.

I personally feel lucky to have been blessed with two advisers, my co-guide Dr. Prem Pal with whom I have worked for the past 4 years. One thing I have observed in him is the fact that he is never wrong about anything, something, which has continued to amaze me over and over. I whole heartedly thank him for introducing me to the feild of MEMS and being patient with me in the nascent stage when I used to ask silly doubts. He was always kind enough for discussions be it on skype or in his office, for hours which has always been fruitful. I also thank him for helping me whenever I was in need of anything. I collectively thank my advisers for teaching me the research ethics along the way. I also thank them for instilling in me the ability of writing the manuscript in a scientific and clear manner. I would also like to thank my committe menbers Dr. Venkatesham and Dr. Jyotsnendu for giving their valuable time for evaluating my work and enlightining me with their knowledge and comments.

I would also like to thank my friends Raaz, Ankush, Harsh, Anjishnu, Tarun, Vishal, Yash and many more for their endless support and encouragement. All my friends who have always been happy on my acheivements and have been with me during my tough days. I would also like to thank my lab mates Ashok, Prashant, Shantanu, Vamshi, Mukul, Aparna. It was a good learning experience working with you guys in the lab.

I would also like to acknowledge the anonymous reviewers of *Journal of Applied Physics, ASME Journal of Vibrations and Accoustics, Journal of Micromechanics and Microengineering, Micro and Nano Systems Letters* for reviewing the papers and giving constructive feedback which helped in improving the manuscript. I would also like to acknowledge the financial support received from Ministry of Human Resource Development (MHRD) and Science and Engineering Research Board (SERB), Government of India towards my Masters education and travel to Delft, The Netherlands for attending the 13th International Conference on Nanomechanical Sensing, respectively.

Finally, above all, I would like to thank my parents Mr. Rakesh Singh and Mrs. Shashi Singh and my brother Sunny Raaj. The freedom they gave me is something I really appreciate and will be indebted to them lifelong. I also thank my father for inculcating in me the desire to study science, he was the first inspiration for me. I thank the almighty God for being with me in all the ups and downs of my life and blessing me. My late grandmother who could not be alive to see me complete my graduation but who always blessed me in every step of my life.

Last but not the least, I would like to thank Late Dr. A.P.J. Abdul Kalam sir, my childhood hero for being an inspiration right from my childhood days.

Dedicated to IIT Hyderabad for all the beautiful minds I met here!

Abstract

Microelectromechanical systems (MEMS) based cantilever beams have been widely used in various sensing applications. Most of the studies concerning these micro/nano resonators are centered around uniform cantilever beams. In this thesis, another class of micro-resonators consisting of non-uniform cantilever beams is investigated. Two classes of beams, one with increasing cross sectional area from the clamped edge (diverging beam) and other with decreasing cross sectional area from the clamped edge (converging beam) are studied. Within each class, beams with linear as well as quartic variation in width are investigated. Firstly, the Euler beam equation for non-uniform cantilever beams considering large deflection and their corresponding exact mode shapes from the linear equation are obtained. Subsequently, using the Galerkin method based on single mode approximation, static and dynamic modal equations for finding pull-in voltage and resonance frequency as a function of DC voltage, respectively are obtained. The research in this thesis is focused around investigating different characteristics including the pull-in voltage, resonance frequency at zero and finite DC voltage, mass sensitivity, size effects, etc. of non-uniform cantilever beams.

The analysis is presented when these microbeams operate in the linear regime about different static equilibriums. In this thesis, we term this frequency as 'linear frequency'. Calculation of the linear frequency is done at different static equilibriums corresponding to different DC voltages. It is found that linear frequency of converging beams increases with increase in non-uniform parameter (α) while those of diverging beams decreases with α. A similar trend is observed for pull-in voltage. Within the converging class, beams with quartic variation in width show significant increase in both frequency and pull-in voltage as compared to corresponding linearly tapered beams. In quantitative terms, converging beams with quartic variation in width and $\alpha = -0.6$ showed an increase in linear frequency by a factor of 2.5 times, and pull-in voltage by 2 times as compared to commonly used uniform beams. Our investigation can prove to be a step forward in designing highly sensitive MEMS sensors and actuators.

Mass sensors are another important MEMS sensors which are widely used in biomedical applications. For detecting small biomolecules, highly sensitive mass sensors are required. Previous studies have aimed at increasing the sensitivity of biomass sensors by reducing the size of cantilever to nanoscale. However, the influence of non-uniform cantilever beam on mass sensitivity has rarely been investigated. In this thesis, the mass sensitivity of linear and nonlinear response of non-uniform cantilever beam with linear and quartic variation in width is also analyzed. To do the analysis, the governing partial differential equation for non-uniform cantilever beam with non-linear curvature effect is used. Subsequently, we obtain the mode shape with tip mass and linear frequency, following which nonlinear response using multiple scale method are obtained. Analysis of linear response indicates that the non-dimensional mass sensitivity increases by ten and fifty times corresponding to first and third mode of a non-uniform converging beam with quartic variation in width. Similarly, the frequency shift of peak amplitude of nonlinear response for a given non-dimensional tip mass increases exponentially and decreases quadratically with tapering parameter, α, for diverging and converging non-uniform beam with quartic variation in width respectively. For the converging beam, an interesting monotonically decreasing and increasing behavior of mass sensitivity with tapering parameter α giving an extremum point at $\alpha = 0.5$ is found. Overall analysis indicates a potential application of the non-uniform beam with quartic converging width for biomass sensor.

As the dimensions of the beam reduces to micro/nano scales, the size-effects becomes profound.

These size-effects alters the dynamic characteristics significantly. As a result, for accurate results, size related effects must be incorporated. However, the continuum theory fails to capture such effects and as a result non-local theories have been developed which can capture the size-effects. Modified strain gradient elasticity theory (MSGT) theory comprises of three additional material length scale parameter to effectively capture the size effect. In this work, beams with fixed-fixed, simply supported and fixed-free boundary conditions are analyzed using MSGT. Additionally, frequency analysis for beams based on the modified coupled stress theory and classical theory is also presented by neglecting one or more length scale parameters. Results obtained for various theories in the present analysis are compared with those available in the literature. To do the above analysis, Differential Quadrature Method (DQM) is used to solve the equations. Two different techniques in order to implement various boundary conditions is also discussed. It is shown that the frequencies based on strain gradient theory are larger as predicted by the modified couples stress theory and the classical theory when the thickness of the beams becomes comparable to the length scale parameter. When the thickness of beams becomes larger than the length scale parameter, the difference in frequencies from different theories diminishes. As a result, size effects are smaller for thicker beams irrespective of the boundary conditions.

Contents

Chapter 1

Introduction

1.1 Motivation

Microelectromechanical systems (MEMS) and nanoelectromechanical systems (NEMS) structures are extensively used in sensors and actuators for myriad applications in various industries. As the name indicates these are constituted of electrical as well as mechanical elements which when combined makes it suitable for application. The electrical aspects includes electrical circuits and power for various actuation methods; electronics for signal processing and control etc. At the same time, the mechanical aspects includes the mechanical vibrating elements or mechanisms the motion of which generates the signal. Fabrication of MEMS devices includes deposition of thin films, lithography, etching, etc. Finally integration of all these in the form of devices are done. As a result, this field is inherently interdisciplinary.

MEMS devices has many advantages, one of them is the batch fabrication which reduces the cost of these devices. Owing to the small size, large scale integration on chips are also possible. MEMS based devices are used as sensors like inertial sensors (e.g. gyroscopes), pressure, temperature, gas sensors etc. and actuators like RF switches, micromirrors etc. which are used in the field of medical science, communication, automobiles, defense and many others.

MEMS based oscillators are one active of research across the world owing to its use in various applications. Mass sensors uses resonating structures to sense the addition of mass, airbags in automobiles uses oscillating structures to sense the change the acceleration. Other devices like temperature sensors, pressure sensors and many others also employs resonating structures. RF MEMS used in communication industries also uses oscillating components. As a result oscillating sensors has proved to be the backbone of sensing devices in MEMS. Scientists have also developed high frequency devices and are exploring new domains such as quantum mechanics. One class of such oscillating sensors are the resonant sensors in which the structures oscillates at its resonance frequency. Any external noise in the form of addition of mass, change in temperature, humidity etc. results in a change of either the mass of the resonating element or the surface stiffness and leads to a change in its resonance frequency. In the coming subsections the application of these resonant sensors and their actuation mechanisms are discussed.

1.1.1 Electrostatically actuated MEMS

There exists different actuation mechanism for MEMS devices including electromagnetic, piezoelectric , electrothermal, electrostatic, etc. Each of these actuation mechanism has its own merit and is used as per the application. Electrostatic actuation is one of the popular means of actuation in MEMS industry owing to its low power consumption, fast response time, ease of integration with CMOS technology and more importantly its compatibility with the existing fabrication methodology. In this actuation methodology, electrostatic forces are induced by creating a potential difference between the electrodes, one of which is the vibrating mechanical element and the other is the fixed bottom electrode. Since, this method of actuation relies on electric field as a result the vibrating element should be good conductor of electricity. With an increase in applied voltage, increased electrostatic forces leads to increased displacement. For application in resonant sensors and other sensors, an AC voltage is superimposed to a DC bias. While the AC voltage induces vibrations, the DC voltage is used for frequency tuning as will be explained later. Electrostatic actuation has a limited operation range called the pull-in voltage. Pull-in voltage is the threshold voltage at which the attractive forces overcomes the restoring spring forces as shown in Fig. 1.1. On application of voltage, the electrostatic force tends to attract cantilever towards fixed electrode, however, the spring force (stiffness) of cantilever resists this force. With further increase in voltage, electrostatic force dominates and the beam is pulled towards fixed electrode. This voltage at which restoring force could no longer balance attractive electrostatic force is known as pull-in voltage. Thus, determination of pull-in voltage is extremely important before designing and operating the device. Another major advantage of electrostatic actuation is the flexibility to tune the frequency by applying a finite DC voltage on top of the alternating AC signal. Since, electrostatic forces are softening in nature, as a result, the frequency of beams reduces under the application of DC voltage.

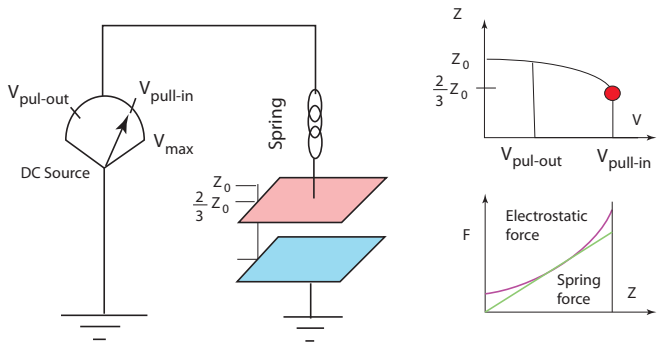

Figure 1.1: Schematic diagram showing the effect at pull-in voltage. As can be seen that as the electrostatic force increase and finally overcomes the spring force, the mechanical element gets pulled-in towards the fixed bottom electrode. This phenomenon is called pull-in and the voltage at which pull-in occurs is known as pull-in voltage.

Another important aspect of electrostatic actuation is the fringing field effect. Fringing effect occurs when the electric field extends the overlapping area of the electrodes. Since the electric field cannot disappear abruptly outside the overlapping area, as a result they form fringes at the edges as shown in Fig. 1.2.

Fringing effect increases when the width of the beam becomes comparable to that of the distance with the bottom electrode.

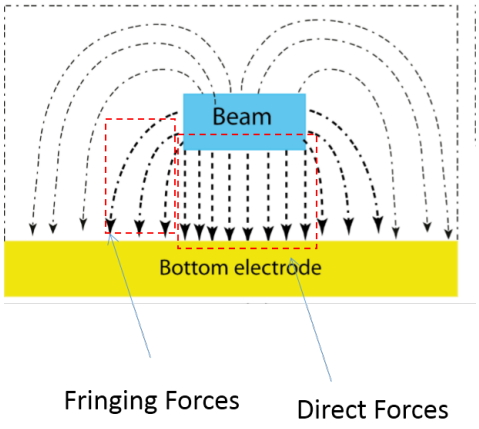

Figure 1.2: Schematic diagram showing the direct and fringing effects.

1.1.2 MEMS based mass sensors

As discussed, performance of most of the MEMS and NEMS based resonant sensors and actuators are dependent on their linear and nonlinear dynamic characteristics near their resonance frequency. To detect the presence of bio-molecules, cantilever based resonant MEMS mass sensors are extensively used. The tip of the cantilever is selectively functionalized to capture the target molecule. When the bio-molecules attaches itself to the cantilever tip, the resonance frequency (by virtue of k or m) of the beam changes as shown in figure 1.3(a). The measurement of this change in the resonance frequency is the principle of MEMS based resonant mass sensors. Here, a mass δm attached at the tip of the cantilever beam with an effective mass m_{eff} is related to the resonance frequency f_0 and the shift in the resonance frequency δf_0 (due to added mass) as [2]

$$\delta m = \frac{2m_{\text{eff}}}{f_0}\delta f_0 = R^{-1}\delta f_0. \tag{1.1}$$

Here, R is the mass responsitivity and, δm is the minimum detectable mass. A high value of R implies better sensitivity. Thus, the sensitivity can be improved by increasing the resonance frequency of the cantilever beam. Another class of MEMS mass sensors operates in the static mode. When the target molecules attached itself to the tip of the beam, there is an associated change in surface stress. This change in the surface stress bends the cantilever. The measurement of deflection of the cantilever tip is the principle of stress based mass sensors. The tip deflection can either be measured optically using laser diode or electrically using piezoresistors.

The above stated mass sensors can operate only in the linear regime. However, the nonlinear behavior of the beams can also be used to detect target molecules. During large amplitude oscillation the frequency response is either of softening type or hardening type due to higher order spring nonlinearities. In both these cases, the symmetrical bell shaped frequency response obtained in the linear regime is distorted as can be seen in Figure 1.3(b). At the same time, these nonlinear response is also characterized by sudden jumps in otherwise continuous response. This sudden jumps in the response is utilized in the detection of target molecules unlike the shift in frequency (or deflection changes) as in the linear case. The resonator is operated near one of the critical point A as shown in Figure 1.3(b). When the target molecules gets attached, the frequency of the beam reduces

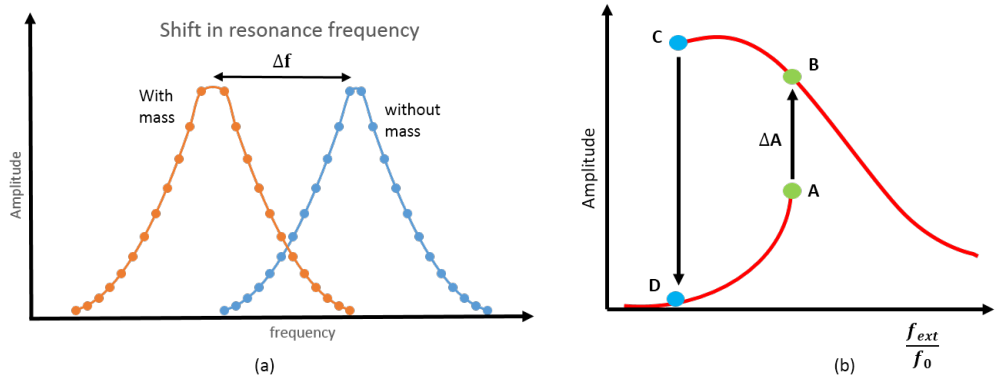

Figure 1.3: Sensing mechanism of linear and nonlinear mass sensors. Amplitude frequency graph of (a) linear mass sensor showing the frequency shift due to addition of tip mass, (b) nonlinear response showing the change in amplitude due to addition of tip mass.

and this results in a sudden increase in amplitude as shown in Figure 1.3(b). The measurement of the amplitude shift can be done using laser vibrometer and is a principle of mass sensing in this case. This method of sensing is very sensitive to small quantities which on one hand increases its sensitivity while on the other exciting the beam at a critical point makes the task difficult as a small disturbance could lead to erroneous results.

1.1.3 Size-effects in MEMS

When the dimensions of mechanical elements like beams, plates, membranes etc. decreases to micro or nano scale, the size effects becomes profound and the mechanical characteristics changes significantly. This has been backed by both experimental and atomistic simulations. While experiments are not always convenient to do as it requires laboratory with sophisticated set-ups; atomistic simulations are quite computationally expensive. As a result, development of theoretical model to study the size-effects for application in MEMS/NEMS is important. The classical beam theory is inherently a scale free theory as a result it fails to capture the size effects. As a result, non-classical theories like the non-local theory, the modifies coupled stress theory (MCST), the modified strain gradient elasticity theory (MSGT) etc. have been developed which contains additional length scale parameters to capture the size related effects.

The non-local theory due to Erigen's nonlocal elasticity theory states that the stress at a material point is a function of strains at all other points of the body. It leads to a fourth order partial differential equation with a nonlocal parameter which consists of a internal characteristic length (lattice parameter, granular size etc). The modified coupled stress theory (MCST) and the modified strain gradient elasticity theory (MSGT) are other non-classical theories which comprises of one and three additional length scale parameters respectively. MSGT is a higher order beam theory which incorporates higher order bending rigidity to effectively capture the size related effects.

1.2 Contribution and outline of thesis

The Euler-Bernoulli beam equation for non-uniform beams considering nonlinearities due to curvature effect is derived using Hamilton's principle. Following which, an analytical method to find the linear exact mode shape for non-uniform beams is discussed. Using this mode shape, the effect of non-uniformity (in width) of cantilever beams on both frequency and pull-in voltage under the influence of DC bias is analysed. Apart from that, potential application of non-uniform beams as MEMS mass sensors is also explored. An analytical model of non-uniform cantilever beams with tip masses is developed which is validated by FEM analysis using ABAQUS. The effect of non-uniformity and the magnitude of tip masses on the linear and nonlinear frequency response is analysed. Finally, the effect of size related effects on the dynamic characteristics of microbeams is discussed using the equation of motion governed by modified strain gradient elasticity theory which is solved using differential quadrature method.

Chapter 1 of this thesis is a comprehensive introduction to different works carried out in this thesis. Background of the concepts and terminologies used in this work is explained. This includes an introduction to MEMS and its application in various domains. Following which a discussion on electrostatically actuated beams is presented including the definition of various terms commonly used in this thesis. Next, the application of cantilever beams as MEMS mass sensors is discussed along with the both linear and nonlinear sensing mechanisms. Finally, the nonlocal theories which incorporates the size-effects in low dimensional beams is discussed.

Chapter 2 starts with a thorough literature survey of the previous work done towards pull-in voltages of different beams. Following which, the derivation of Euler-Bernoulli beam equation for non-uniform beams considering nonlinearity is presented. Next, the methodology of obtaining the exact mode shape for non-uniform beams by transforming the governing equation of non-uniform beams to that of an equivalent uniform beam is discussed. Next, the static and dynamic equations using Gelarkin's method is obtained. Finally, the effect of non-uniformity in width on the pull-in voltage of electrostatically actuated cantilever beams is discussed. At the same time, the advantage of non-uniform beams in frequency tuning is also discussed.

In **chapter 3**, MEMS based mass sensors based on non-uniform beams are investigated. The effect of both non-uniformity as well as tip masses on the linear and nonlinear behavior is discussed. The effect of tip masses on linearly tapered beams is also compared to that of other numerical solutions available in open literature. Additionally, Finite element simulation is also carried out using ABAQUS to obtain the modal frequencies with and without tip masses to validate the analytical model. The method of multiple scales (MMS) is used to solve the nonlinear governing equation to obtain the nonlinear frequency response and to study the effect of tip mass as well as non-uniformity on the frequency.

In **chapter 4**, we discuss the size-effects and its effect on the dynamics of micro beams. The modified strain gradient elasticity theory which comprises of additional length scale parameters to capture the size-effects is solved using differential quadrature method. The modal frequencies corresponding to this theory is obtained and compared with the classical continuum theory as well as other non-classical theories like modified stress gradient theory. The changes in modal frequencies when non-classical theories are used is discussed for beams with different end conditions.

In the last chapter we present the conclusions of our thesis and a discussion on the future scope of this thesis.

Chapter 2

Electrostatically actuated non-uniform cantilever beams

2.1 Introduction

Electrostatically actuated MEMS cantilever beams form an excellent class of resonator for various devices. Most of these resonant MEMS/NEMS devices such as mass sensor, temperature sensor, pressure sensor, etc., [2, 3, 4] operate at resonance frequency of the structure. In order to improve performance of MEMS devices, tuning of the resonance frequency has caught attention of researchers in the past [5, 6, 7, 8]. Attempts have been made to tune frequency of cantilever beams by reducing the dimensions to nano scale [9], using nonlinear effect to soften or harden the system [6, 7, 8, 10] etc. Therefore, it is vital to compute an accurate resonance frequency of such resonators during their design phase. Apart from computing resonance frequency, knowledge of pull-in voltage is also important to achieve stable operating range [6]. A system of cantilever beam separated from the bottom electrode by a gap d_0 forms a parallel plate capacitance system as shown in Fig. 2.1(a).

Researchers in the past have modeled resonators and obtained pull-in parameters by accounting various effects [11, 12, 13, 14, 15, 16, 17]. However, these models are limited to uniform cantilever beams. At the same time a few studies are performed for the computation of frequencies of non uniform cantilever beams as well [19, 20, 21]. Mabie *et al* [19] and Lau [20] obtained linear frequency of double tapered beam with tip mass by expressing the mode shape in terms of Bessel functions. In yet another study, Mabie and Roger [21] analyzed beam with constant width and linearly tapered thickness using same methodology. At the same time, special cases of tapering were also studied by William *et al* [22] on axially loaded beams, Auciello *et al* [23] by obtaining solution in terms of Bessel Function, and Wang [24] with the help of hypergeometric functions. For MEMS and NEMS applications, tapering in width (rather than thickness) is of interest as it is pertinent to microfabrication techniques where arbitrary planar geometry (with constant thickness) can be fabricated with existing methods. In this regard, Mabie *et al* [21] and Wang [25] numerically integrated the differential equation corresponding to beam with varying width alone and obtained the frequency for various taper parameters. Abrate [26] proposed a method to transform the linear governing equation for special type of nonuniform width to that of a uniform beam by introducing a function. In this chapter, we focus on non-uniform cantilever beam and investigate the effect of non-uniformity on

frequency as well as pull-in voltage of non-uniform cantilever based resonators. In present study, we have used the transformation proposed by Abrate to find mode shape based on linear equation, however, we use this mode shape to study influence of nonlinear curvature effect due to large DC voltage on linear frequency of non-uniform cantilever beam using Galerkin approach.

To compute pull-in voltage in MEMS, several authors have worked towards obtaining its closed form expression. Nathonson *et al* [11] obtained simplest form of pull-in voltage expression by modeling the cantilever beam as a lumped spring-mass system considering uniform gap. To include the effect of non-uniform gap between beams due to deflection with respect to fixed electrode, Pamidighantam *et al* [12] included the effects of partial electrodes, axial stress, non-linear stiffening, charge-redistribution, fringing fields etc., to obtain closed form expression for pull-in voltage. Osterberg *et al* [13] proposed another closed form expression for pull-in voltage including the corrections based on finite element simulations. Chowdhury *et al* [27] obtained a closed form model for calculating the pull in voltage based on capacitance formula given by Mejji and Fokkema [28]. Later, Kalaiarasi *et al* [29] found that the model obtained by Chowdhury *et al* [27] is limited to a range of selective dimensions. Consequently, they proposed closed form models based on different capacitance models available in literature to calculate pull-in voltage. After validating the models with Finite Element Analysis (FEA) based software, they concluded that different capacitance models have to be used for different ranges of beam dimensions. Later Tilman *et al* [14] used minimum energy principle to discuss pull in instability of clamped-clamped beam. To include the effect of large deformation, Chaterjee *et al* [30] numerically studied variation of pull-in instability for uniform cantilever beam considering the effect of large deflection. Li *et al* [31] performed pull-in analysis in the linear, nonlinear and mixed regime of MEMS fixed-fixed as well as cantilever beams. Based on their analysis, they concluded that different theories should be used for beams with different configurations and dimensions. A similar study was performed by Rasekh *et al* [32] to do pull-in analysis of carbon nanotube based cantilever beams. Rahaeifard *et al* [33] used modified coupled stress theory to capture the size effect on pull-in voltage of a nanoscaled beam. Subsequently, Baghani [34] included nonlinear geometric effects along with size effect to obtain the pull in voltage. However, most of the above studies were limited to uniform beams. To capture fringing effect due to non-uniform shape of the fixed electrode, Cheng *et al* [35] studied pull-in parameters of rectangular cantilever torsion actuator due to electrostatic actuation with respect to elliptical, hyperbolic and parabolic electrodes. Similarly, Lemaire *et al* [36], Raulli *et al* [37] and Abdalla *et al* [38] worked towards optimizing geometry and studied its effect on pull-in parameters. Najar *et al* [39, 40] employed differential quadrature method to study pull-in parameters of beam with varying thickness, width and distance from the fixed bottom electrode. Another study by Joglekar and Pawaskar [41] focused on the dynamic and static pull-in analysis of linearly tapered cantilever beams using numerical technique. Almost all studies concerning non-uniform beams (fixed-fixed and cantilever) have resorted to using numerical techniques or other transformation methods to find the pull-in voltage. In this chapter, we present pull-in voltage and frequency analysis of non-uniform cantilever beams with varying widths and nonlinear curvature effect by using Galerkin method based on the exact mode shape of linear non-uniform cantilever beam.

2.2 Analytical modeling: Equation of motion

In this section, we derive governing equation of transverse motion $w(x,t)$ along z direction considering large deflection for nonuniform cantilever beam under the influence of electrostatic force Q_s as shown in Fig. **??**. To derive the equation, we consider a cantilever beam of length L, width $b(x)$, thickness h, area moment of inertia $I(x)$, density ρ and effective modulus $E = \frac{E'}{(1-v^2)}$, where E' is the Young's modulus and v is the Poisson's ratio.

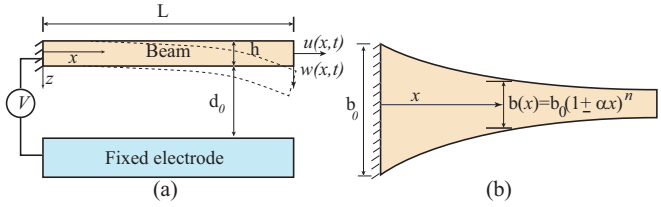

Figure 2.1: (a) Transverse vibration of a cantilever beam subjected to electrostatic excitation. (b) Variation of width of a non-uniform cantilever beam with tapering parameter α as $b(x) = b_0(1+\alpha x)^n$, where, $n = 1$ and 4 imply beam with linear and quartic taper in width, respectively. Here, $\alpha < 0$ corresponds to converging beam, $\alpha > 0$ corresponds to diverging beams and $\alpha = 0$ implies uniform beam. Given figure depicts a quartic converging beam with $\alpha < 0$ and n=4.

2.2.1 Derivation of nonlinear governing equation for non-uniform beams

If $u(x,t)$ is an axial extension under large deflection, then the axial strain ζ_{xx} at neutral axis can be written as [42]

$$\zeta_{xx} = \sqrt{\left(1 + \frac{\partial u(x,t)}{\partial x}\right)^2 + \left(\frac{\partial w(x,t)}{\partial x}\right)^2} - 1 \tag{2.1}$$

and the curvature k as [43]

$$k = \left(1 + \frac{\partial u}{\partial x}\right)\frac{\partial^2 w}{\partial x^2} - \frac{\partial^2 u}{\partial x^2}\frac{\partial w}{\partial x}. \tag{2.2}$$

Writing the kinetic energy KE and bending strain energy U_s as

$$KE = \frac{1}{2}\int_0^L \rho A(x)\{\dot{u}^2 + \dot{w}^2\}dx$$

$$U_s = \frac{1}{2}\int_0^L EI(x)k^2 dx.$$

and then using the virtual work done by external force such that $\delta Q = Q_s$, we apply Hamilton's principle

$$\int_{t_1}^{t_2} (\delta KE - \delta U_s - \delta Q)dt = 0, \tag{2.3}$$

to obtain the governing equation. After substituting the energy expression and using an approximate expression of $u' = -w'^2/2$ under inextensibility condition, i.e., $\zeta_{xx} = 0$, the governing equation with

non-linear terms upto $O(\epsilon^3)$ for undamped forced vibration can be written as

$$\rho A(x)\ddot{w} - EI(x)(w^{''})^3 + w^{'}\rho A(x)\int_0^x (w'\ddot{w}' + (\dot{w}^{'})^2)dx + w'(EI(x)w''w')'' + (EI(x)w'')'' = Q_s(t) \tag{2.4}$$

where, $Q_s(t)$ is the electrostatic force considering fringing field effect which is given by [41]

$$Q_s(t) = \frac{1}{2}\frac{\epsilon_0 b(x)(V+v(t))^2}{(d_0-w)^2}\left(1+\frac{2(d_0-w)}{\pi b(x)}\right). \tag{2.5}$$

where, $\epsilon_0 = 8.854\times10^{-12}$ F/m is the permittivity of free space, V is DC voltage and $v(t)$ is AC voltage.
The boundary conditions for non-uniform cantilever beam can be written as

$$w(0) = \frac{\partial w}{\partial x}|_{x=0} = 0,\ \frac{\partial^2 w}{\partial x^2}|_{x=L} = 0,\ \frac{\partial}{\partial x}\left(EI(x)\frac{\partial^2 w}{\partial x^2}\right)|_{x=L} = 0. \tag{2.6}$$

2.2.2 Non-dimensionalisation

To obtain non-dimensional form of governing equation given by Eqn. (2.4) and boundary conditions given by Eqn. (2.6), we define following non-dimensional parameters,

$$x^* = \frac{x}{L},\ w^* = \frac{w}{d_0},\ t^* = \frac{t}{(L^2\sqrt{\frac{\rho A_0}{EI_0}})}, \gamma = \frac{d_0}{L},\ f_1(x) = \frac{E\tilde{I}(x)}{EI_0},\ f_2(x) = \frac{\rho\tilde{A}(x)}{\rho A_0}, \tag{2.7}$$

where, $EI(x) = EI_0 + E\tilde{I}(x) = (1+f_1(x))EI_0$ and $\rho A(x) = \rho A_0 + \rho\tilde{A}(x) = (1+f_2(x))\rho A_0$, I_0 and A_0 are the area moment of inertia and cross-sectional area at the fixed end of cantilever beam, respectively. We substitute nondimensional parameters in Eqns. (2.4) and (2.6) rearrange the terms to get the equivalent non-dimensional governing equation as (after dropping the superscript * for convenience)

$$(1+f_2(x))\ddot{w} + ((1+f_1(x))w^{''})^{''} - \gamma^2(1+f_1(x))(w^{''})^3 + \gamma^2(1+f_3(x))w^{'}\int_0^x((\dot{w}^{'})^2 + w^{'}\ddot{w}^{'})dx + \gamma^2 w^{'}\times((1+f_1(x))w^{''}w^{'})^{''} - \frac{1}{2}\frac{\epsilon_0 b(x)(V+v(t))^2 L}{\gamma^3 EI_0(1-w)^2} - \frac{\epsilon_0(V+v(t))^2L^2}{\pi\gamma^2 EI_0(1-w)} = 0 \tag{2.8}$$

and the boundary condition as

$$w(0) = \frac{\partial w}{\partial x}|_{x=0} = 0,\ \frac{\partial^2 w}{\partial x^2}|_{x=1} = 0, \frac{\partial}{\partial x}(1+f_1(x))\frac{\partial^2 w}{\partial x^2}|_{x=1} = 0 \tag{2.9}$$

In the following section, we obtain exact mode shape from linear undamped equation under free vibration corresponding to uniform as well as non-uniform beams.

2.2.3 Linear mode shape for non-uniform beams

In this section, we obtain exact mode shape of cantilever beam with uniform as well as linear and quartic tapering in width. To obtain the mode shape, we consider governing equation under linear,

undamped and free vibration conditions, thus, neglecting the nonlinear, damping and forcing terms. After substituting the expressions for f_1 and f_2 in Eqn. (2.8), the resulting linear equation for non-uniform beam can be written as

$$\frac{\partial^2}{\partial x^2}\left(\big(EI(x)\big)\frac{\partial^2 w}{\partial x^2}\right) + \frac{EI_0}{\rho A_0}(\rho A(x))\frac{\partial^2 w}{\partial t^2} = 0. \tag{2.10}$$

To obtain mode shape, we convert the equation for non-uniform beam into an equivalent governing equation of uniform beam by following the approach as proposed by Abrate [27]. Taking a function $\sigma(x)$ such that $v(x) = \sigma(x)w(x)$, the equation for uniform beam can be written as

$$\frac{\partial^4(\sigma w)}{\partial x^4} + \frac{\partial^2(\sigma w)}{\partial t^2} = 0. \tag{2.11}$$

Writing the expanded form of Eqns. (2.10) and (2.11) as

$$(I^{''}w^{''} + Iw^{''''} + 2I^{'}w^{'''}) + \frac{I_0}{A_0}A(x)\ddot{w} = 0 \tag{2.12}$$

and

$$(\sigma^{''''}w + 4\sigma^{'''}w^{'} + 6\sigma^{''}w^{''} + 4\sigma^{'}w^{'''} + \sigma w^{''''}) + \sigma\ddot{w} = 0, \tag{2.13}$$

and then comparing the terms on left hand side of Eqns. (2.12) and (2.13), we get following relationship

$$\frac{6\sigma^{''}}{I^{''}} = \frac{4\sigma^{'}}{2I^{'}} = \frac{\sigma}{I} = \frac{A_0\sigma}{I_0A(x)}. \tag{2.14}$$

Taking $\sigma(x)$ such that $\sigma^{''''}$ and $\sigma^{'''}$ are either zero or negligible, and satisfying Eqn. (2.14), we find σ, $I(x)$ and $A(x)$ corresponding to each type of tapered beam, separately. Consequently, for computed form of σ, $I(x)$ and $A(x)$, Eqn. (2.10) for non-uniform beam and Eqn. (2.11) for uniform beam with $v(x) = \sigma w$ become equivalent. Based on equivalent uniform beam, the exact mode shape for Eqn. (2.11) is readily available as [44]

$$v(x) = A_1\sin(\lambda x) + A_2\cos(\lambda x) + A_3e^{\lambda x} + A_4e^{-\lambda x}. \tag{2.15}$$

Finally, mode shape of non-uniform beam with given tapering can be found from the relation $w(x) = \frac{v(x)}{\sigma(x)}$ on which the boundary conditions as given by Eqn. (2.9) can be applied to find the constants. For a uniform beam the boundary conditions can be applied to obtain the mode shape given by

$$v(x) = \sigma(x)w(x) = A_1[\sin(\lambda x) - \sinh(\lambda x) - \frac{\sin(\lambda) + \sinh(\lambda)}{\cos(\lambda) + \cosh(\lambda)}(\cos(\lambda x) - \cosh(\lambda x))]. \tag{2.16}$$

In the following section, we apply above concept in computing mode shapes of uniform and non-unform beams with different types of tapering and mention the frequency equation to obtain corresponding frequency parameter, λ.

Frequency equation

- Uniform beams

  For uniform cantilever beam, we get $\sigma(x) = 1$, $A(x) = A_0$, and $I(x) = I_0$. Consequently, for $v(x) = w(x)$, mode shape is given by Eqn. (2.16). Using appropriate boundary conditions, value of frequency parameter λ can be numerically obtained by solving the following transcedental equation

$$2\lambda^6(2 + e^{\lambda}\cos(\lambda) + e^{-\lambda}\cos(\lambda)) = 0. \tag{2.17}$$

- Beams with linear variation in width

  For a non-uniform cantilever beam with linearly tapered width, $b(x) = b_0(1 + \alpha x)$, where, $-1 < \alpha < 0$ corresponds to converging type and $\alpha > 0$ corresponds to diverging case. The area moment of inertia and area can be written as $I(x) = I_0(1 + \alpha x)$ and $A(x) = A_0(1 + \alpha x)$, respectively. The corresponding expression of σ can be obtained from Eqn. (2.14) as $\sigma(x) = \sqrt{(1 + \alpha x)}$, thus, $A(x) = A_0\sigma(x)^2$ and $I(x) = I_0\sigma(x)^2$. Since, the above relationship of σ and α in case of linearly tapered width is obtained by neglecting higher order differential terms σ'''' and σ''', the error associated with such assumptions grows rapidly as $|\alpha| > 0.5$. For given boundary condition, frequency parameter λ can be found from the frequency equation

$$\begin{aligned}
&\frac{\lambda^2}{8(1+\alpha)^4}\big(16\cos(\lambda)e^{\lambda}\alpha^4\lambda^4 + 64\cos(\lambda)e^{-\lambda}\alpha\lambda^4 + 12\cos(\lambda)e^{-\lambda}\alpha^4\lambda + 64\cos(\lambda)e^{\lambda}\alpha\lambda^4 \\
&-12\cos(\lambda)e^{\lambda}\alpha^4\lambda - 48\sin(\lambda)e^{-\lambda}\alpha^2\lambda^3 + 12\sin(\lambda)e^{-\lambda}\alpha^4\lambda + 64\cos(\lambda)e^{-\lambda}\alpha^3\lambda^4 + 96 \\
&\times\cos(\lambda)e^{\lambda}\alpha^2\lambda^4 + 16\cos(\lambda)e^{-\lambda}\alpha^4\lambda^4 + 32\lambda^4 - 6\alpha^4 + 192\alpha^2\lambda^4 + 32\alpha^4\lambda^4 + 128\alpha^3\lambda^4 \\
&+128\alpha\lambda^4 + 64\cos(\lambda)e^{\lambda}\alpha^3\lambda^4 + 48\cos(\lambda)e^{-\lambda}\alpha^2\lambda^3 + 16\cos(\lambda)e^{-\lambda}\alpha^4\lambda^3 + 48\alpha^3\lambda^3 \\
&\times e^{-\lambda}\cos(\lambda) - 48\cos(\lambda)e^{\lambda}\alpha^2\lambda^3 - 16\cos(\lambda)e^{\lambda}\alpha^4\lambda^3 - 48\cos(\lambda)e^{\lambda}\alpha^3\lambda^3 + 12e^{\lambda}\sin(\lambda) \\
&\times\alpha^3\lambda + 16e^{-\lambda}\alpha\lambda^3\cos(\lambda) + 12e^{-\lambda}\sin(\lambda)\alpha^3\lambda - 16e^{\lambda}\cos(\lambda)\alpha\lambda^3 + 96\cos(\lambda) \\
&\times e^{-\lambda}\alpha^2\lambda^4 - 12e^{\lambda}\cos(\lambda)\alpha^3\lambda - 16e^{\lambda}\alpha\lambda^3\sin(\lambda) + 12\cos(\lambda)e^{-\lambda}\alpha^3\lambda - 16e^{-\lambda}\sin(\lambda) \\
&\times\alpha\lambda^3 + 16e^{\lambda}\lambda^4\cos(\lambda) + 3e^{\lambda}\alpha^4\cos(\lambda) + e^{-\lambda}16\cos(\lambda)\lambda^4 + 3e^{-\lambda}\alpha^4\cos(\lambda) - 48\sin(\lambda) \\
&\times e^{\lambda}\alpha^2\lambda^3 + 12\sin(\lambda)e^{\lambda}\alpha^4\lambda - 48\sin(\lambda)e^{\lambda}\alpha^3\lambda^3 - 48\sin(\lambda)\lambda^3e^{-\lambda}\alpha^3 - 16e^{\lambda}\sin(\lambda)\alpha^4\lambda^3 \\
&-16\sin(\lambda)e^{-\lambda}\alpha^4\lambda^3\big) = 0
\end{aligned} \tag{2.18}$$

  Finally, for given λ and σ, mode shape can be obtained from $w(x) = \frac{v(x)}{\sigma(x)}$, where, $v(x)$ is given by Eqn. (2.16).

- Beams with quartic variation in width

  For a non-uniform cantilever beam with quartic variation in width, we take $b(x) = b_0(1+\alpha x)^4$, where, $-1 < \alpha < 0$ corresponds to converging type and $\alpha > 0$ corresponds to diverging case. Although, there is no restriction over validity of Eqn. (2.14) in this case, we restrict the value of α to 0.6 for quartic tapered beam. The area moment of inertia and area can be written as $I(x) = I_0(1 + \alpha x)^4$ and $A(x) = A_0(1 + \alpha x)^4$, respectively. Corresponding expression of σ can be obtained from Eqn. (2.14) as $\sigma(x) = (1 + \alpha x)^2$, thus, $A(x) = A_0\sigma(x)^2$ and $I(x) = I_0\sigma(x)^2$.

Frequency parameter λ can be found from the frequency equation

$$\begin{aligned}
&\frac{2\lambda^2}{(1+\alpha)^4}\Big(-12\sin(\lambda)e^{-\lambda}\alpha^4\lambda - 4e^{\lambda}\cos(\lambda)\alpha\lambda^3 - 12e^{\lambda}\sin(\lambda)\alpha^3\lambda + 4e^{-\lambda}\cos(\lambda)\alpha\lambda^3 \\
&+24e^{\lambda}\sin(\lambda)\alpha^3\lambda^2 - 12e^{\lambda}\sin(\lambda)\alpha^2\lambda^3 - 24e^{-\lambda}\sin(\lambda)\alpha^3\lambda^2 - 12e^{-\lambda}\sin(\lambda)\alpha^2\lambda^3 + 12e^{\lambda} \\
&\times\cos(\lambda)\alpha^4\lambda - 12e^{\lambda}\cos(\lambda)\alpha^2\lambda^3 + 4e^{\lambda}\cos(\lambda)\alpha\lambda^4 - 12e^{-\lambda}\cos(\lambda)\alpha^4\lambda + 12e^{-\lambda}\cos(\lambda) \\
&\times\alpha^2\lambda^3 + 4e^{-\lambda}\cos(\lambda)\alpha\lambda^4 + e^{\lambda}\cos(\lambda)\alpha^4\lambda^4 + e^{-\lambda}\cos(\lambda)\alpha^4\lambda^4 - 4e^{\lambda}\sin(\lambda)\alpha^4\lambda^3 - 4e^{-\lambda}\alpha^4 \\
&\times\ \sin(\lambda)\lambda^3 - 4e^{\lambda}\cos(\lambda)\alpha^4\lambda^3 + 4e^{\lambda}\cos(\lambda)\alpha^3\lambda^4 + 4e^{-\lambda}\cos(\lambda)\alpha^4\lambda^3 + 4e^{-\lambda}\cos(\lambda)\alpha^3\lambda^4 \\
&+12e^{\lambda}\sin(\lambda)\alpha^4\lambda^2 - 12e^{\lambda}\sin(\lambda)\alpha^3\lambda^3 - 12e^{-\lambda}\sin(\lambda)\alpha^4\lambda^2 - 12e^{-\lambda}\sin(\lambda)\alpha^3\lambda^3 - 12e^{\lambda} \\
&\times\cos(\lambda)\alpha^3\lambda^3 + 6e^{\lambda}\cos(\lambda)\alpha^2\lambda^4 + 12e^{-\lambda}\cos(\lambda)\alpha^3\lambda^3 + 6e^{-\lambda}\cos(\lambda)\alpha^2\lambda^4 - 12e^{\lambda}\sin(\lambda) \\
&\times\alpha^4\lambda + 12e^{\lambda}\cos(\lambda)\alpha^3\lambda + 12e^{\lambda}\sin(\lambda)\alpha^2\lambda^2 - 4e^{\lambda}\sin(\lambda)\alpha\lambda^3 - 12e^{-\lambda}\cos(\lambda)\alpha^3\lambda - 12e^{-\lambda} \\
&\times\sin(\lambda)\alpha^2\lambda^2 - 4e^{-\lambda}\sin(\lambda)\alpha\lambda^3 + 24\alpha^4 - 12\alpha^3e^{-\lambda}\sin(\lambda)\lambda - 12e^{-\lambda}\cos(\lambda)\alpha^4 + e^{\lambda}\cos(\lambda) \\
&\times\lambda^4 + e^{-\lambda}\cos(\lambda)\lambda^4 - 12e^{\lambda}\cos(\lambda)\alpha^4 + 8\alpha\lambda^4 + 2\alpha^4\lambda^4 + 8\alpha^3\lambda^4 + 12\alpha^2\lambda^4 + 2\lambda^4\Big)\Big) = 0 \quad (2.19)
\end{aligned}$$

Like linearly tapered beam, for given λ and σ, the mode shape can be obtained from $w(x) = \frac{v(x)}{\sigma(x)}$, where, $v(x)$ is given by Eqn. (2.16).

2.3 Analytical modeling: Station and dynamic equations

To determine pull-in voltage and frequency at different DC voltages, we first obtain static and dynamic deflection equations for non-uniform cantilever beams with different tapers. Since the net transverse deflection, $w(x,t)$, is composed of a static deflection $z_s(x)$ due to application of DC bias and dynamic deflection $z(x,t)$ due to AC voltage, $w(x,t)$ becomes

$$w(x,t) = z_s(x) + z(x,t). \quad (2.20)$$

Substituting the assumed deflection in nondimensional governing equation as given by Eqn. (2.8) and setting the time-varying dynamic terms as zero, we obtain equation governing static deflection as

$$\begin{aligned}
&f_1^{''}z_s^{''} + 2f_1^{'}z_s^{'''} + (1+f_1)z_s^{''''} - \gamma^2(1+f_1)(z_s^{''})^3 + \gamma^2 z_s^{'}\Big(f_1^{''}z_s^{''}z_s^{'} + 2f_1^{'}z_s^{'''}z_s^{'} + 2f_1^{'}(z_s^{''})^2 \\
&+(1+f_1)z_s^{''''}z_s^{'} + 3(1+f_1)z_s^{'''}z_s^{''}\Big) - \frac{1}{2}\frac{\epsilon_0 b(x)V^2L}{\gamma^3 EI_0(1-z_s)^2} - \frac{\epsilon_0 V^2L^2}{\pi\gamma^2 EI_0(1-z_s)} = 0. \quad (2.21)
\end{aligned}$$

Similarly, the dynamic equation is obtained by substituting Eqn.(2.20) in Eqn.(2.8), where, the static deflection z_s is obtained from Eqn.(2.21). Expanding the forcing term about $z = 0$ and retaining terms upto first order, we obtain corresponding linear dynamic equation by neglecting the nonlinear

terms, dissipation terms and forcing terms as

$$(1+f_2)\ddot{z}+(1+f_1)z^{''''}+\big(4z_s^{'}z^{''}f_1^{'}\gamma^2+3\gamma^2z_s^{'}f_1z^{'''}+2\gamma^2z_s^{'}f_1^{''}z^{'}+3\gamma^2z^{'}f_1z_s^{'''}$$
$$+3\gamma^2z_s^{'}z^{'''}+3\gamma^2z^{'}z_s^{'''}\big)z_s^{''}+\big((-3\gamma^2f_1-3\gamma^2)(z_s^{''})^2+\gamma^2(z_s^{'})^2f_1^{''}+3\gamma^2z_s^{'}f_1z_s^{'''}$$
$$+3\gamma^2z_s^{'}z_s^{'''}+f_1^{''}\big)z^{''}+\big(2\gamma^2z_s^{'}f_1z_s^{''''}+4\gamma^2z_s^{'}f_1^{'}z_s^{'''}+2\gamma^2f_1^{'}(z_s^{''})^2+2\gamma^2z_s^{'}z_s^{''''}\big)z^{'}$$
$$+\big(\gamma^2f_1z^{''''}+2\gamma^2f_1^{'}z^{'''}+\gamma^2z^{''''}\big)(z_s^{'})^2+\Big(\gamma^2\int_0^x\big(z^{'''}z_s^{'}f_2+z^{'''}z_s^{'}\big)dx\Big)z_s^{'}+2f_1^{'}z^{'''}$$
$$-\frac{\epsilon_0V^2L}{\gamma^2EI_0}\left(\frac{b(x)}{\gamma(1-z_s)^3}+\frac{L}{\pi(1-z_s)^2}\right)z=0 \qquad (2.22)$$

2.3.1 Reduced order model

In order to find reduced order equations, we approximate static and dynamic deflections based on first transverse mode as $z(x,t)=P(t)\phi(x)$ and $z_s=A\phi(x)$, respectively, where, $\phi(x)$ is mode shape of non-uniform cantilever beam with different tapering as obtained in previous sections. However, it is to be noted that for the first flexural mode, static deflection due to applied DC voltage is not very different from mode shape. As a result, static deflection is assumed in terms of the mode shape. However, this approximation is valid only for the first resonance mode. At higher modes, shape of static deflection will no longer be equal to dynamic deflection, i.e., the mode shape. Here, we carried out further analysis only for first resonance mode. Subsequently, we apply Galerkin method to reduce static and dynamic equations given by Eqns. (2.21) and (2.22), respectively, to reduced order form. The reduced form of static equation governing amplitude of static deflection A is given

$$\Big(\int_0^1\big(f_1^{''}\phi(x)^{''}\phi(x)+2f_1^{'}\phi(x)^{'''}\phi(x)+(1+f_1)\phi(x)\phi(x)^{''''}\big)dx\Big)A+\Big(\int_0^1\big(-\gamma^2(1+f_1)$$
$$\times(\phi(x)^{''})^3\phi(x)+\gamma^2(\phi(x)^{'})^2f_1^{''}\phi(x)^{''}\phi(x)+\gamma^2\phi(x)^{'}2f_1^{'}\phi(x)^{'''}\phi(x)^{'}\phi(x)+2\gamma^2f_1^{'}(\phi(x)^{''})^2$$
$$\times\phi(x)\phi(x)^{'}+(1+f_1)\gamma^2(\phi(x)^{'})^2\phi(x)^{''''}\phi(x)+3(1+f_1)\gamma^2\phi(x)^{'}\phi(x)\phi(x)^{'''}\phi(x)^{''}\big)dx\Big)A^3$$
$$-\frac{1}{2}\frac{\epsilon_0V^2L}{\gamma^3EI_0}\int_0^1\Big(\frac{b(x)\phi(x)}{(1-A\phi(x))^2}\Big)dx-\frac{\epsilon_0V^2L^2}{\pi\gamma^2EI_0}\int_0^1\left(\frac{\phi(x)}{(1-A\phi(x))}\right)dx=0 \qquad (2.23)$$

and the dynamic equation becomes

$$\left[\int_0^1(1+f_2)(\phi(x))^2dx\right]\ddot{P}+\left[\int_0^1\left[(1+f_1)\phi(x)^{''''}+\left(\big(4\phi(x)^{'}\phi(x)^{''}f_1^{'}\gamma^2+3\gamma^2\phi(x)^{'}\right.\right.\right.$$
$$\times f_1\phi(x)^{'''}+2\gamma^2\phi(x)^{'}f_1^{''}\phi(x)^{'}+3\gamma^2\phi(x)^{'}f_1\phi(x)^{'''}+3\gamma^2\phi(x)^{'}\phi(x)^{'''}+3\gamma^2\phi(x)^{'}$$
$$\left.\times\phi(x)^{''''}\big)\phi(x)^{''}+\big((-3\gamma^2f_1-3\gamma^2)(\phi(x)^{''})^2+\gamma^2(\phi(x)^{'})^2f_1^{''}+3\gamma^2\phi(x)^{'}f_1\phi(x)^{'''}\right.$$
$$+3\gamma^2\phi(x)^{'}\phi(x)^{'''}+f_1^{''}\big)\phi(x)^{''}+\Big(\gamma^2\int_0^x\phi(x)^{'''}\phi(x)^{'}f_2+\phi(x)^{'''}\phi(x)^{'}\big)dx\Big)\phi(x)^{'}+$$
$$\Big(\big(2\gamma^2\phi(x)^{'}f_1\phi(x)^{''''}+4\gamma^2\phi(x)^{'}f_1^{'}\phi(x)^{'''}+2\gamma^2f_1^{'}(\phi(x)^{''})^2+2\gamma^2\phi(x)^{'}\phi(x)^{''''}\big)\phi(x)^{'}+$$
$$\left.\big(\gamma^2f_1\phi(x)^{''''}+2\gamma^2f_1^{'}\phi(x)^{'''}+\gamma^2\phi(x)^{''''}\big)(\phi(x)^{'})^2\Big)\right)A^2+2f_1^{'}\phi(x)^{'''}$$
$$\left.-\frac{\epsilon_0V^2L}{\gamma^2EI_0}\left(\frac{b(x)\phi(x)}{\gamma(1-A\phi(x))^3}+\frac{L}{\pi}\frac{\phi(x)}{(1-A\phi(x))^2}\right)\right]\phi(x)dx\Bigg]P=0. \qquad (2.24)$$

In subsequent sections, we obtain pull-in voltage and frequency variation of first transverse mode of non-uniform beams.

2.3.2 Normal mode frequency

To find frequency of first transverse mode of the system, we re-write Eqn.(2.24) of dynamic deflection in following form,

$$M\ddot{P} + KP = 0. \tag{2.25}$$

Consequently, the frequency ω of oscillating cantilever beam about statically deflected position due to applied DC voltage is given by

$$\omega = \sqrt{\frac{K}{M}}. \tag{2.26}$$

On comparing Eqns. (2.24) and (2.25), we get the expression for M and K in terms of amplitude of static deflection A, DC Voltage V, beam dimensions and properties as

$$M = \int_0^1 (1 + f_2)(\phi(x))^2 dx$$

and

$$\begin{aligned} K = \int_0^1 \Bigg[& (1+f_1)\phi(x)^{''''} + \Big(\Big(4\phi(x)^{'}\phi(x)^{''} f_1^{'}\gamma^2 + 3\gamma^2\phi(x)^{'} f_1\phi(x)^{'''} + 2\gamma^2\phi(x)^{'} f_1^{''}\phi(x)^{'} + 3\gamma^2\phi(x)^{'} \\ & \times f_1\phi(x)^{'''} + 3\gamma^2\phi(x)^{'}\phi(x)^{'''} + 3\gamma^2\phi(x)^{'}\phi(x)^{'''} \Big)\phi(x)^{''} + \Big((-3\gamma^2 f_1 - 3\gamma^2)(\phi(x)^{''})^2 + \gamma^2(\phi(x)^{'})^2 f_1^{''} \\ & + 3\gamma^2\phi(x)^{'} f_1\phi(x)^{'''} + 3\gamma^2\phi(x)^{'}\phi(x)^{'''} + f_1^{''} \Big)\phi(x)^{''} + \Big(\gamma^2 \int_0^x \phi(x)^{'''}\phi(x)^{'} f_2 + \phi(x)^{'''}\phi(x)^{'} \Big) dx \Big)\phi(x)^{'} \\ & + \Big(\big(2\gamma^2\phi(x)^{'} f_1\phi(x)^{''''} + 4\gamma^2\phi(x)^{'} f_1^{'}\phi(x)^{'''} + 2\gamma^2 f_1^{'}(\phi(x)^{''})^2 + 2\gamma^2\phi(x)^{'}\phi(x)^{''''} \big)\phi(x)^{'} + \big(\gamma^2 f_1\phi(x)^{''''} \\ & + 2\gamma^2 f_1^{'}\phi(x)^{'''} + \gamma^2\phi(x)^{''''} \big)(\phi(x)^{'})^2 \Big) \Big) A^2 + 2f_1^{'}\phi(x)^{'''} \\ & - \frac{\epsilon_0 V^2 L}{\gamma^2 E I_0} \left(\frac{b(x)\phi(x)}{\gamma(1 - A\phi(x))^3} + \frac{L}{\pi}\frac{\phi(x)}{(1 - A\phi(x))^2} \right) \Bigg] \phi(x) dx \end{aligned} \tag{2.27}$$

Finally, it is important to note that frequency equation considers nonlinear curvature effect which becomes important at large static deflection under large DC voltage. Any nonlinearity in the motion amplitude of AC component, leading to so-called Duffing resonance, is not considered in this work.

2.3.3 Pull-in voltage

Pull-in voltage is the DC voltage at which electrostatic force becomes equal to elastic force. Consequently, static deflection of beam approaches to infinite when the voltage increases beyond pull-in voltage, i.e., $\frac{dA}{dV}|_{V=V_{\rm PI}} \to \infty$ or $\frac{dV}{dA}|_{V=V_{\rm PI}} = 0$. Therefore, in order to obtain pull-in voltage, we

differentiate the reduced form of static equation given by Eqn.(2.23) with respect to A to get

$$\Big(\int_0^1 \big(f_1^{''}\phi(x)^{''}\phi(x)+2f_1^{'}\phi(x)^{'''}\phi(x)+(1+f_1)\phi(x)\big)\phi(x)^{''''}dx\Big)+3\Big(\int_0^1\big(-\gamma^2(1+f_1)\phi(x)\times(\phi(x)^{''})^3+\gamma^2(\phi(x)^{'})^2f_1^{''}\phi(x)^{''}\phi(x)+\gamma^2\phi(x)^{'}2f_1^{'}\phi(x)^{'''}\phi(x)^{'}\phi(x)+2\gamma^2\phi(x)^{'}f_1^{'}\times(\phi(x)^{''})^2\phi(x)+(1+f_1)\gamma^2(\phi(x)^{'})^2\phi(x)\phi(x)^{''''}+3(1+f_1)\gamma^2\phi(x)\phi(x)^{'}\phi(x)^{''}\phi(x)^{'''}\big)dx\Big)A^2-\frac{\epsilon_0 L}{\gamma^2EI_0}\Bigg[\frac{V}{\gamma}\frac{dV}{dA}\int_0^1\Big(\frac{b(x)\phi(x)}{(1-A\phi(x))^2}\Big)dx+\frac{V^2}{\gamma}\int_0^1\Big(\frac{b(x)\phi(x)^2}{(1-A\phi(x))^3}\Big)dx+\frac{2LV}{\pi}\frac{dV}{dA}\times\int_0^1\Big(\frac{\phi(x)}{(1-A\phi(x))}\Big)dx+\frac{LV^2}{\pi}\times\int_0^1\Big(\frac{\phi(x)^2}{(1-A\phi(x))^2}\Big)dx\Bigg]=0. \quad (2.28)$$

After substituting $\frac{dV}{dA}|_{V=V_{\rm PI}}=0$ for the condition at pull-in, we obtain the following expression of pull-in voltage

$$V_{\rm PI}=\left[\frac{\gamma^2EI_0}{\epsilon_0 L}\frac{S}{E}\right]^{\frac{1}{2}}, \quad (2.29)$$

where,

$$E=\left[\frac{1}{\gamma}\int_0^1\Big(\frac{b(x)\phi(x)^2}{(1-A_{\rm PI}\phi(x))^3}\Big)dx+\frac{L}{\pi}\int_0^1\Big(\frac{\phi(x)^2}{(1-A_{\rm PI}\phi(x))^2}\Big)dx\right]$$

and

$$S=\int_0^1\Big[f_1^{''}\phi(x)^{''}\phi(x)+2f_1^{'}\phi(x)^{'''}\phi(x)+(1+f_1)\phi(x)\phi(x)^{''''}\Big]dx+3A_{\rm PI}^2\times\int_0^1\Big[-\gamma^2(1+f_1)(\phi(x)^{''})^3\phi(x)+\gamma^2(\phi(x)^{'})^2f_1^{''}\phi(x)^{''}\phi(x)+\gamma^2\phi(x)^{'}2f_1^{'}\phi(x)^{'''}\times\phi(x)^{'}\phi(x)+2\gamma^2\phi(x)^{'}f_1^{'}(\phi(x)^{''})^2\phi(x)+(1+f_1)\gamma^2(\phi(x)^{'})^2\phi(x)^{''''}\phi(x)+3(1+f_1)\times\gamma^2\phi(x)^{'}\phi(x)\phi(x)^{'''}\phi(x)^{''}\Big]dx,$$

where, $A_{\rm PI}$ is the static deflection at pull-in voltage. Static deflection from Eqn. (2.23) at pull-in parameters is solved along with Eqn. (2.29) to obtain the pull-in voltage.

2.4 Results and discussion

In this section, we discuss the effect of non-uniformity parameter, α, on above mentioned phenomenon for the uniform beam as well as beams with linear and quartic taper in width. Again, we mention that $\alpha>0$ and $-1<\alpha<0$ correspond to diverging and converging beams, respectively. The uniform beam corresponds to the case when $\alpha=0$. In the first subsection, we first validate the modal frequencies with those obtained from finite element analysis . Subsequently, we discuss the effect of taper parameter on linear frequency at zero DC voltage, when nonlinear curvature effect is negligible for different beams. Next, we use the linear mode of different tapered beams to obtain pull-in voltage and frequency of non-uniform cantilever beam with nonlinear curvature effects. Fi-

nally, we compare results with available values in literature for some cases and then discuss about the importance of tapering.

2.4.1 Numerical modeling using ABAQUS

In order to check the robustness of the presented analysis, modal analysis of beams with different shapes were performed using finite element based software ABAQUS. The beam geometry was created using a python script which was capable of creating a solid model of various planar geometry and different thickness. Eight elements were taken in the direction of thickness to ensure convergence. The first three frequencies and the mode shape obtained from ABAQUS were then compared with our analytical model as well as the results obtained by other authors using numerical integration of the governing equations [15]. The results are in good agreement with both the results obtained from ABAQUS as well as those available in open literature. The first three mode shapes for different types of non-uniform beams are shown in Fig. 2.2. In the next section, we tabulate the comparison of modal frequencies in order to validate our approach.

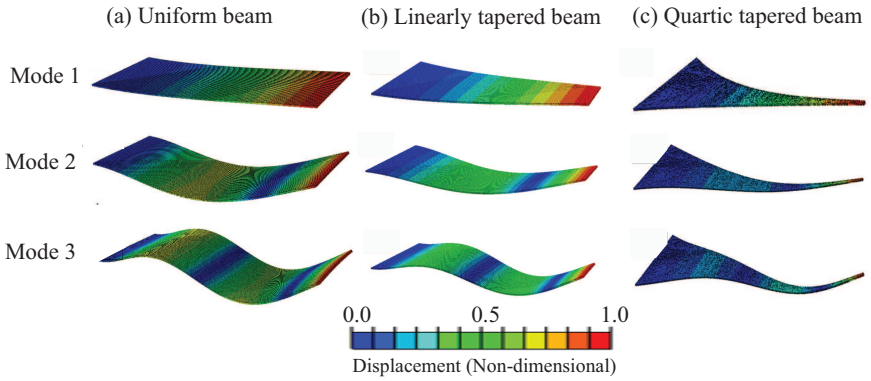

Figure 2.2: Mode shapes of first three beams for (a) uniform beam, (b) linear tapered beam and (c) quartic tapered beam obtained from ABAQUS.

2.4.2 Frequency analysis at zero DC voltage

The transcendental Eqns. (2.17), (2.18), and (2.19) corresponding to the uniform beam, beams with linear tapers and beams with quartic taper respectively, can be solved numerically to obtain reso-

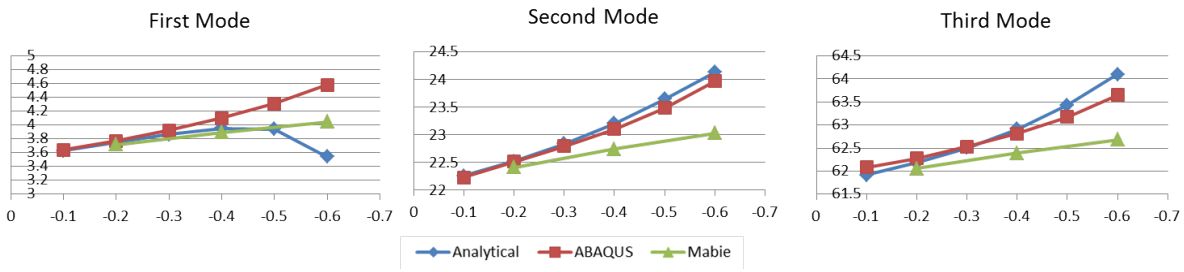

Figure 2.3: Comparison of first three frequencies for beams with linear variation in width for different α obtained from the presented analytical mode, ABAQUS and that of Mabie [21].

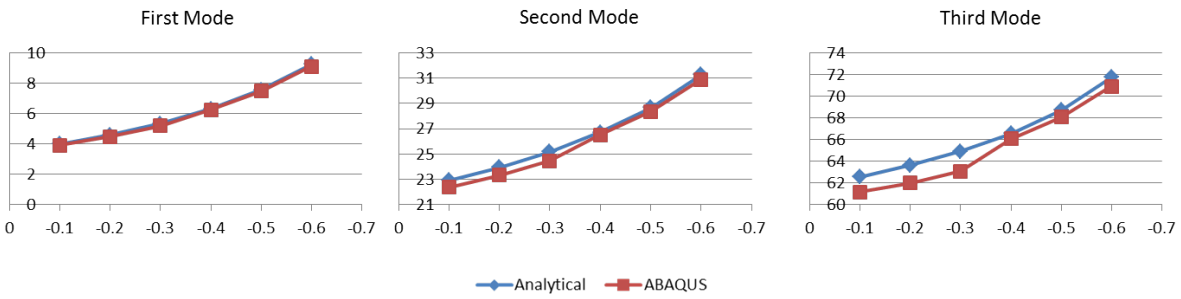

Figure 2.4: Comparison of first three frequencies for beams with quartic variation in width for different α obtained from the presented analytical mode and ABAQUS

nance frequencies for different α. These equations can be used to obtain frequencies for higher modes as well. Fundamental frequencies for all the three cases for various α are tabulated in Tables 2.1 and 2.2, where, $\alpha = 0$ corresponds to uniform beam. Results for uniform and linearly converging beams are also compared with that obtained from ABAQUS and those obtained by Mabie *et al* [15] using numerical integration without finding the mode shape. As previously mentioned, transformation of linearly tapered beam into equivalent uniform beam is done with some approximation. The effect of this approximation can be observed from Table 2.1 as well as Fig. 2.3. However, this transformation for quartic case is done exactly without any approximation. This can be validated by the excellent agreement obtained with FEM simulations as presented in Fig. 2.4. By comparing the computed results with available results, we get percentage errors of 1.5% and 12.5% corresponding to taper parameter, α, -0.4 and -0.6, respectively. Additionally, we have found that for $alpha = -0.5$, percentage error in computing pull-in voltage from the proposed method is less than 1% or 2% when compared with FEM or semianalytical solution as mentioned by Joglekar and Pawaskar [41] in Table 2.4. Therefore, the approximation considered in non-uniform beam with linear taper in width gives negligible error when $|\alpha| \leq 0.4$, the percentage error for $0.5 \leq |\alpha| \leq 0.6$ can be assumed to be less than 12.5%. Thus, the approach adopted in this chapter is validated and can be extended to compute frequencies of non-uniform beams with different tapering. Figure 2.5 shows variation of linear frequency with α for both converging and diverging beams with linear and quartic taper in width. We observe that frequency for diverging beams decreases with an increase in α, while that of a converging beam increases. For converging beam with quartic taper in width, the frequency is about 2.5 times greater than that of a uniform beam. The corresponding mode shape can be obtained for different beams for given values of α as discussed earlier. As a result, application of non-uniform cantilever beam (in particular beams with quartic variation in width) can prove to be an excellent means in improving the performance of resonant sensors and actuators which operate at resonance frequency. In subsequent subsections, we discuss the pull-in voltage and resonance frequency of various non-uniform beams by including the non-linear curvature effect.

2.4.3 Frequency analysis at finite DC voltage

To study vibration of different types of cantilever beams under the application of DC voltage, we solve static deflection Eqn.(2.23) at different V to get static deflection A. Using obtained value of A, we find frequency from Eqn.(2.26) for different values of DC voltage. Figure 2.6 shows variation

Table 2.1: The non dimensional fundamental frequency of converging (negative α) and diverging (positive α) beam with linear taper in width.

α	Present	Mabie *et al.* [15]	ABAQUS
0.0	3.516	3.516	3.529
-0.1	3.628	–	3.642
-0.2	3.747	3.717	3.771
-0.3	3.865	–	3.922
-0.4	3.954	3.892	4.098
-0.5	3.940	–	4.312
-0.6	3.540	4.048	4.578

α	Present
0.0	3.516
0.1	3.413
0.2	3.321
0.3	3.237
0.4	3.162
0.5	3.096
0.6	3.036

Table 2.2: The non dimensional frequency of converging (negative α) and diverging (positive α) beam with quartic tapering in width

α	Present	ABAQUS
0.0	3.516	3.529
-0.1	3.994	3.902
-0.2	4.587	4.466
-0.3	5.336	5.178
-0.4	6.298	6.240
-0.5	7.558	7.466
-0.6	9.235	9.906

α	Frequency
0.0	3.516
0.1	3.124
0.2	2.799
0.3	2.526
0.4	2.294
0.5	2.096
0.6	1.924

of the frequency with applied DC voltage for various types of beams. Frequencies are normalized with their corresponding frequencies at zero DC voltage. From figure 2.6, we see that increase of DC voltage causes the system to soften and frequency decreases with an increase in voltage. We know that geometrical non-linearity has stiffening effect while inertial nonlinearity and linear electrostatic forces have softening effect. However, overall effect on the dynamics depends on relative strength of each nonlinearity. In our analysis, we have neglected higher order terms of dynamic deflection in order to obtain linear frequency at finite DC voltage. With an increase of applied DC voltage, linear frequency is found to decrease, thus, the system undergoes softening effect due to linear electrostatic forces. This trend is obtained as the initial gap to beam length ratio (γ) is less than 0.3 where the stiffening effect of geometrical nonlinearity is minimal. For $\gamma > 0.3$ and higher DC voltage, the combined effect of geometrical nonlinearity and nonlinear electrostatic force with higher order terms becomes inevitable [32]. While this study considers geometrical nonlinearity in analysis, the higher order nonlinear terms of electrostatic forces are neglected.

2.4.4 Pull-in analysis

To obtain pull-in voltage for different tapered beams by following the approach as explained earlier, we first validate our model for pull-in voltage of a uniform beam with five different results from the literature as mentioned in Table 2.3. Taking dimensions and material properties for each case as: (1) $L = 20000$ μm, $b = 5000$ μm, $h = 57$ μm, $d_0 = 92$ μm, $E' = 155.8$ GPa, $v = 0.06$; (2) $L = 20000$ μm, $b = 5000$ μm, $h = 57$ μm, $d_0 = 92$ μm, $E' = 155.8$ GPa, $v = 0.06$; (3) $L = 100$ μm, $b = 50$ μm, $h = 3$ μm, $d_0 = 1$ μm, $E' = 169$ GPa, $v = 0.06$; (4) and (5) $L = 300$ μm, $b = 50$ μm, $h = 1$ μm, $d_0 = 2.5$ μm, $E' = 77$ GPa, $v = 0.33$, computed results from the developed model are found to be

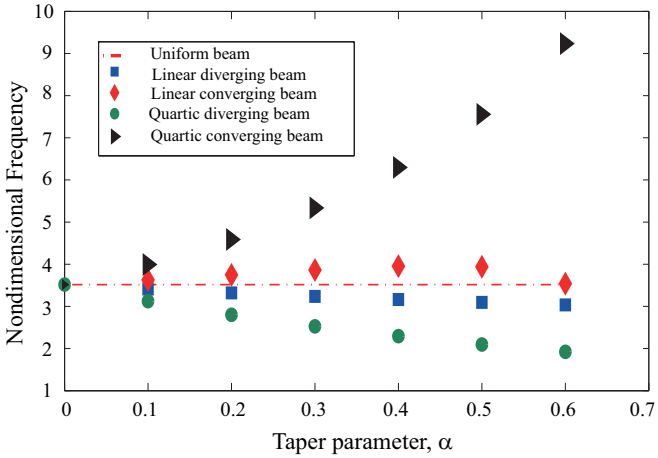

Figure 2.5: Effect of taper parameter (α) on the linear frequency for various cases of tapering

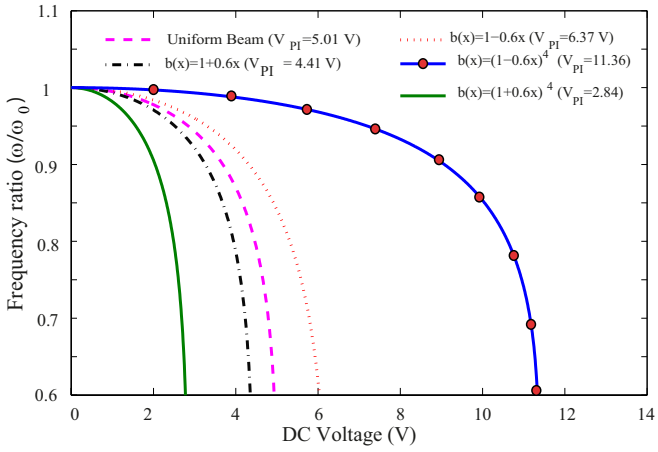

Figure 2.6: Variation of linear, non-dimensional frequency with applied DC voltage for various types of beams. ω_0 is the frequency at zero DC voltage

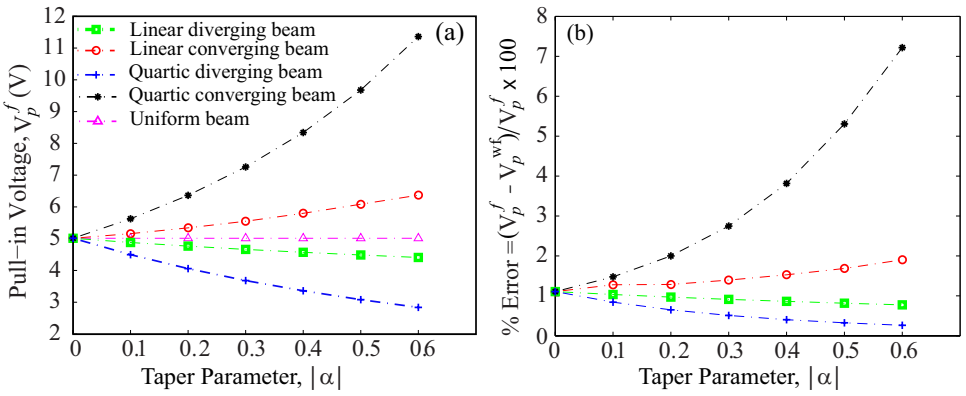

Figure 2.7: (a) Effect of taper parameter (α) on pull-in voltage V_p^f including fringing effects for various cases of tapering; (b) Variation of percentage error in computing pull-in voltage with fringing effect, V_p^f, and without fringing effect, V_p^{wf}, with taper parameter.

in good agreement with available results. To compare the accuracy of non-uniform beam, when α is non-zero, we take few cases of converging beam with linear variation in width and compare the results with that of Joglekar and Pawaskar [41] in Table 2.4. The dimensions and material properties for case (1) and (2) are taken as $L = 200$ μm, $b = 40$ μm, $h = 1$ μm, $d_0 = 2$ μm, $E' = 169$ GPa, $v = 0.06$, and that of (3) and (4) are taken as $L = 100$ μm, $b = 15$ μm, $h = 1\mu$m, $d_0 = 2$ μm, $E' = 169$ GPa, $v = 0.06$. On comparing the pull-in voltage of linearly tapered beam for $\alpha = -0.25$

Table 2.3: Comparison of the pull-in voltage of uniform cantilever beam with existing literature

Sample Number	$V_{\text{Pull-in}}$ (V) (Present model)	$V_{\text{Pull-in}}$ (V) (Reference)	Reported By (method)
1	65.19	68.5	Hu *et al* [45] (experimental)
2	65.19	66.78	Chaterjee & Pohit [30] (numerical)
3	37.15	37.84	Chowdhury *et al* [27] (numerical)
4	2.23	2.27	Chowdhury *et al* [27] (numerical)
5	2.23	2.29	Joglekar & Pawaskar [41] (analytical)

Table 2.4: Comparison of pull-in voltage of converging beam with linearly tapered width with existing literature

Sample Number	α	Pull-in voltage by present model (V)	Pull-in voltage by Joglekar and Pawaskar [41] (V)
1	-0.25	5.45	5.59 (analytical)
2	-0.25	5.45	5.61(FEA)
3	-0.5	24.74	24.26(analytical)
4	-0.5	24.74	24.68(FEA)

and -0.5 obtained from the present method with the results from Joglekar and Pawaskar [41] in Table 2.4, we get percentage error of about 2%. Although nonlinear curvature effect is neglected in their models, it may be insignificant for the given geometry. Now, we extend the analysis to different types of tapered beams. Figure 2.7(a) shows pull-in voltage with different taper parameters (α) for beams with linear and quartic variation in width. The dimensions and material properties for each case are taken as $L = 200$ μm, $b = 40$ μm, $h = 1$ μm, $d_0 = 2$ μm, $E' = 168.39$ GPa, $v = 0.06$. Figure 3.6(b) shows comparison of percentage difference in computing the pull-in voltage with and without fringing field effects of different non-uniform beams at different taper parameters. For a quartic tapered beam with taper parameter of $\alpha = -0.6$, we get a maximum percentage difference of about 7%. From our analysis, we find that for a converging beam, the pull-in voltage increases with an increase in α, while for diverging beam, it decreases. This trend was expected because of the changes in stiffness of converging and diverging beam with α. Similar changes were also observed in case of linear frequency in previous section. The linear frequency for diverging beam decreases with an increase in α which implies that stiffness effect (or spring force) decreases. As a result, at

a lower voltage, electrostatic forces balance the spring force, and then the pull-in occurs. While in case of converging beam, frequency (or stiffness) is more, and as a result a higher voltage is needed for electrostatic forces to overcome the spring force offered by cantilever beam. Consequently, we see that pull-in voltage increases by more than 100% in case of converging beam with quartic tapering as compared to uniform beam. Thus, employing a cantilever beam with quartic variation in width gives us a larger voltage threshold which is about 2 times as that of a widely used uniform beam for the operation of MEMS devices.

2.5 Conclusions

In this chapter, we have developed theoretical model for computing the frequency as well as pull-in voltage of non-uniform cantilever beam with nonlinear curvature effects. The non-uniformity considered in this chapter is for the cantilever beams with linear and quartic tapering in width. To develop this model, we first obtained the exact mode shape from linear equation for beams with different non-uniformities. Subsequently, we apply the Galerkin method based on single mode shape to find the formulation for pull-in voltage and frequency from corresponding static and dynamic equations respectively. From our analysis, we have observed that linear frequency can be increased by more than 2.5 times, whereas, pull-in voltage can also be increased by 2 times simply by varying the order of tapering in the quartic tapered beam. Such findings can be utilized not just to increase the sensitivity of cantilever based devices, but it also increases the operating range of bias voltage.

Chapter 3

Mass sensors based on non-uniform beams

3.1 Introduction

Microelectromechanical systems (MEMS) and nanoelectromechanical systems (NEMS) components are an integral part of many resonant sensors and actuators in the domains of biomedical [46, 47], automobiles [48], communication [49] etc. as already discussed in Chapter 1. Most of the biomass sensors use either uniform cantilever beam or uniform clamped-clamped beam as a sensing element. Since, the sensitivity of a typical cantilever biomass sensor is directly proportional to the resonance frequency and the quality factor, there have been various efforts in increasing the stiffness by reducing the size of beam to nanoscale [47] and increasing the quality factor by modifying the design [46]. It has also been noticed that the performance of mass sensor can be improved by utilizing the nonlinear dynamics of uniform cantilever beam with tip mass [50, 51]. In this chapter, we investigate the non-uniform variation of the width of a cantilever beam with added mass on its linear and nonlinear frequency response.

There have been several studies associated with the linear and nonlinear vibrations of uniform beams [50, 52, 53] as well as non-uniform beams [54, 55, 56]. Mabie and Roger [54] studied the vibrations of cantilever beams with linearly tapered thickness by obtaining the solution in terms of known Bessel functions and linearly tapered width using numerical integration. At the same time double tapered cantilever beams have been studied by Mabie *et al* [55] and Lau [56] with tip mass, again by obtaining the mode shape in terms of known Bessel functions. Additionally, beam with special cases of tapering have been studied by obtaining the solution in terms of the Bessel Function by Auciello *et. al* [22], and hypergeometric functions by Wang [58]. William *et. al* [59] has studied the influence of symmetrically linear and parabolic tapered sections on the resonance frequency of axially loaded beams. Abrate [26] solved the linear governing equation for special type of non-uniform width which can be transformed into equivalent equation of uniform beam. However, his study neglected the nonlinear effect. Recently, Wang [60] has numerically obtained the frequency of a tapered cantilever beam of constant thickness and linearly tapered width. A close examination of the above studies reveal that many of these studies include the investigation of the linear frequency of beam with tapered thickness [54], beam with both linearly tapered thickness and width [55, 56],

etc. However, the studies related with the linear frequency of a beam with varying width are limited [26, 54, 60], perhaps, due to the difficulties in obtaining the exact form of the solution in this case. Moreover, the nonlinear curvature effect is also neglected in [26, 54, 60].

To improve the performance of cantilever based mass sensor, Kacem *et al* [51] have studied the performance of a mass sensor based on nonlinear dynamics. Ouakad and Younis [53] studied the nonlinear response of clamped-clamped and cantilever carbon nanotube considering geometrical non-linearities. Kim *et al* [50] dealt with a cantilever based mass sensor with added mass considering both geometrical as well as inertial nonlinearities. There are several other studies [61, 62, 63] which are related with the nonlinear dynamics of uniform cantilever beam. To study the nonlinear response of non-uniform beam, Jaber *et al* [64] presented the non-linear vibration of double tapered cantilever beam with elastically restrained end to investigate the effect of tapering on the nonlinear behavior at the first, second and third modes. Katsikadelis *et al* [65] studied the non-linear dynamics of beam with variable stiffness and non-linear boundary conditions using the analog equation method. Karimpour *et al* [66] studied the nonlinear dynamics of non-uniform beam with doubly tapered section using energy balance method and harmonic balance method. Most of the above studies are associated with either double tapering along the width and thickness or tapering along the thickness. Clementi *et al.* [67] performed nonlinear dynamical studies of non-uniform simply-supported beam subjected to axial and transverse loading. Moreover, these studies employ linearly tapered section without considering the tip mass. In this analysis, we deal with the non-linear dynamics of non-uniform cantilever having linear and quartic tapered width with tip mass. Moreover, the study related with variability in width is important due to possible constraints in fabricating microcantilever beam with double tapered section or a section with tapered thickness.

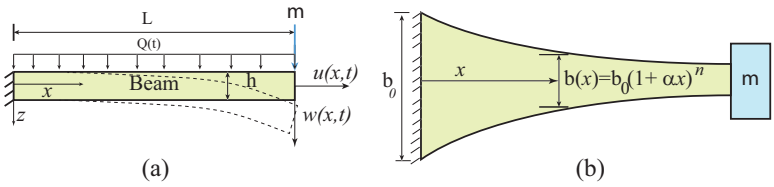

Figure 3.1: (a) Transverse vibration and axial stretching of a cantilever beam under uniformly distributed load. (b) The beam geometry used in our analysis. α=0 corresponds to a uniform beam, $\alpha > 0$ corresponds to diverging beam and $\alpha < 0$ corresponds to converging beams. Furthermore, n = 1 implies beam with linear variation in width and n = 4 implies beam with quartic variation in width.

3.2 Analytical modeling: Equation of motion

To develop the analytical model, we use the nonlinear Euler beam equation governing the transverse vibration of a non-uniform cantilever beam with sinusoidal forcing given by [68].

$$\rho A(x)\ddot{w} - EI(x)(w^{''})^3 + w^{'}\rho A(x)\int_0^x (w'\ddot{w}' + (\dot{w}^{'})^2)dx + w'(EI(x)w''w')'' + (EI(x)w'')'' + c\dot{w} = Q(t) \tag{3.1}$$

where, c is the viscous damping coefficient, $Q(t) = F\sin(\Omega t)$ is the uniformly applied load as shown in Fig. 3.1 and over-dots and over-dash refers to differentiation with respect to time and space respectively. Using the non-dimensional parameters

$$x^* = \frac{x}{L},\ w^* = \frac{w}{L},\ t^* = \frac{t}{(L^2\sqrt{\frac{\rho A_0}{EI_0}})}, f_1(x) = \frac{E\tilde{I}(x)}{EI_0}, f_2(x) = \frac{\rho\tilde{A}(x)}{\rho A_0}, \tag{3.2}$$

such that $EI(x) = EI_0 + E\tilde{I}(x) = (1 + f_1(x))EI_0$, $\rho A(x) = \rho A_0 + \rho\tilde{A}(x) = (1 + f_2(x))\rho A_0$, where, I_0 and A_0 are the area moment of inertia and cross sectional area at the fixed end of the cantilever beam respectively, we get the equivalent non-dimensional governing equation as (after dropping * for convenience)

$$\begin{aligned}&(1 + f_2(x))\ddot{w} + ((1 + f_1(x))w^{''})^{''} - (1 + f_1(x))(w^{''})^3 + (1 + f_2(x))w^{'} \times \\ &\int_0^x ((\dot{w}^{'})^2 + w^{'}\ddot{w}^{'})dx + c_1\dot{w} + w^{'}((1 + f_1(x))w^{''}w^{'})^{''} - \frac{L^3F}{EI_0}\sin(\Omega t) = 0.\end{aligned} \tag{3.3}$$

The corresponding boundary conditions with added tip mass can be written as

$$w(0,t) = \left.\frac{\partial w(x,t)}{\partial x}\right|_{x=0} = 0,\ \left.\frac{\partial^2 w(x,t)}{\partial x^2}\right|_{x=1} = 0,\ \left.\frac{\partial}{\partial x}\Big(1 + f_1(x)\frac{\partial^2 w(x,t)}{\partial x^2}\Big)\right|_{x=1} = \mu\frac{\partial^2 w(1,t)}{\partial t^2} \tag{3.4}$$

where, $\mu = \frac{m}{\rho A_0 L}$, m is the added tip mass and $c_1 = \frac{cL^2}{\sqrt{\rho A_0 EI_0}}$.

3.2.1 Mode shape and boundary conditions

In this section, we find the linear mode shape for different beams as done in Chapter 2. We repeat the technique for easy reference. To find the linear undamped mode shape, we remove the nonlinear and damping terms of Eqn. (3.3) to obtain the linear governing equation for transverse vibrations, w_{nu}, of non-uniform beams. Since, the exact analytical solution of the resulting equation for a beam with tapered width is difficult to obtain, we introduce a function $\sigma(x)$ and convert equation for non-uniform equation to an equivalent equation for a uniform beam in terms of $w_u = \sigma w_{nu}$ as described in [26, 68]. By equating the coefficients of non-uniform and uniform equations, we find the expression of $\sigma(x)$, where, the higher derivative terms of σ such as $\sigma^{''''}$, $\sigma^{'''}$, are either zero or negligible. We use the single mode approximation as $w_u(x,t) = \phi_u(x)\eta(t)$ and $w_{nu}(x,t) = \phi_{nu}(x)\eta(t)$, where ϕ_u and ϕ_{nu} are the mode shapes for uniform and non-uniform beams, respectively to obtain the resulting equation. The solution of this equation gives the mode shape which is solved with boundary condition from Eqn. (3.4) to obtain the modal frequencies and mode shapes for different types of beams. For a uniform beam, $(\sigma(x) = 1)$ the mode shape after applying the boundary conditions is

$$\begin{aligned}\phi_u(x) = A_1\Bigg[\Lambda\Bigg(&(2\cos(\lambda)\cosh(\lambda)\lambda\mu + \cos(\lambda)\sinh(\lambda) + \sin(\lambda)\cosh(\lambda))\sin(\lambda x) \\ &+(2\cos(\lambda)\sinh(\lambda)\lambda\mu + 1 + \cos(\lambda)\cosh(\lambda) + \sinh(\lambda)\sin(\lambda))\cosh(\lambda x) \\ &-(2\cos(\lambda)\cosh(\lambda)\lambda\mu + \cos(\lambda)\sinh(\lambda) + \sin(\lambda)) \\ &\times\cosh(\lambda)\sinh(\lambda x)\Bigg) + \cos(\lambda x)\Bigg]\end{aligned} \tag{3.5}$$

where, $\Lambda = \Big[-\sin(\lambda)\Big(2\lambda\mu\cosh(\lambda)+\sinh(\lambda)\Big)+\cos(\lambda)\cosh(\lambda)+1\Big]^{-1}$ and μ is the tip mass parameter. The mode shape is dependent on the tip mass μ. The value of constant A_1 can be found by normalizing the mode shape using the relation $\int_0^1 \phi^2 dx = 1$.

Using similar methodology, we obtain the mode shape for non-uniform beams which effectively becomes $\phi_{nu} = \frac{\phi_u(x)}{\sigma(x)}$, where, $\sigma(x)$ is a function which captures the non-uniform effect in mode shape [68]. For a beam with linear variation in width, $\sigma(x) = \sqrt{1+\alpha x}$ and for quartic variation in width, $\sigma(x) = (1+\alpha x)^2$. The boundary conditions given in Eqn. (3.4) are applied on the mode shape $\phi_{nu}(x)$ to obtain the corresponding frequency equations. Subsequently, the frequency equation is solved numerically to obtain the different frequencies of the beams.

3.2.2 Frequency equation

- Uniform beams For uniform cantilever beam, we get $\sigma(x) = 1$, $A(x) = A_0$, and $I(x) = I_0$. Consequently, for $v(x) = w(x)$ the mode shape is given by Eqn. (3.5). Using the appropriate boundary conditions, the value of frequency parameter λ can be obtained by numerically solving the following transcendental equation for a given value of added tip mass parameter μ

$$2\lambda^6(e^{\lambda}\cos(\lambda)\lambda\mu - e^{\lambda}\sin(\lambda)\lambda\mu - e^{\lambda}\cos(\lambda)\lambda\mu - e^{-\lambda}\sin(\lambda)\lambda\mu + 2 + e^{\lambda}\cos(\lambda) + e^{-\lambda}\cos(\lambda)) = 0. \tag{3.6}$$

- Beams with linear variation in width

For a tapered cantilever beam with linearly tapered width $b(x) = b_0(1+\alpha x)$, the area moment of inertia and area can be written as $I(x) = I_0(1+\alpha x)$ and $A(x) = A_0(1+\alpha x)$, respectively. The corresponding expression of σ can be obtained from Eqn. (2.14) as $\sigma(x) = \sqrt{(1+\alpha x)}$, thus, $A(x) = A_0\sigma(x)^2$ and $I(x) = I_0\sigma(x)^2$. The frequency parameter λ can be found from the

frequency equation

$$\frac{\lambda^2}{8(1+\alpha)^4}\left(16\cos(\lambda)e^{\lambda}\alpha^4\lambda^4+64\cos(\lambda)e^{-\lambda}\alpha\lambda^4+12\cos(\lambda)e^{-\lambda}\alpha^4\lambda+64\cos(\lambda)e^{\lambda}\alpha\lambda^4\right.$$
$$-12\cos(\lambda)e^{\lambda}\alpha^4\lambda-48\sin(\lambda)e^{-\lambda}\alpha^2\lambda^3+12\sin(\lambda)e^{-\lambda}\alpha^4\lambda+32\alpha^3\lambda^4\mu+64\alpha^2\lambda^4\mu$$
$$+48\cos(\lambda)e^{\lambda}\alpha\lambda^5\mu+16\cos(\lambda)e^{\lambda}\alpha^3\lambda^5\mu+64\cos(\lambda)e^{-\lambda}\alpha^3\lambda^4+96\cos(\lambda)e^{\lambda}\alpha^2\lambda^4$$
$$+16\cos(\lambda)e^{-\lambda}\alpha^4\lambda^4+32\lambda^4-6\alpha^4+192\alpha^2\lambda^4+32\alpha^4\lambda^4+128\alpha^3\lambda^4+128\alpha\lambda^4$$
$$+64\cos(\lambda)e^{\lambda}\alpha^3\lambda^4+48\cos(\lambda)e^{-\lambda}\alpha^2\lambda^3+16\cos(\lambda)e^{-\lambda}\alpha^4\lambda^3+48\cos(\lambda)e^{-\lambda}\alpha^3\lambda^3$$
$$-48\cos(\lambda)e^{\lambda}\alpha^2\lambda^3-16\cos(\lambda)e^{\lambda}\alpha^4\lambda^3-48\cos(\lambda)e^{\lambda}\alpha^3\lambda^3+12e^{\lambda}\sin(\lambda)\alpha^3\lambda+16e^{-\lambda}$$
$$\times\cos(\lambda)\alpha\lambda^3+12e^{-\lambda}\sin(\lambda)\alpha^3\lambda-16e^{\lambda}\lambda^5\mu\sin(\lambda)-16e^{-\lambda}\sin(\lambda)\lambda^5\mu-16e^{\lambda}\cos(\lambda)$$
$$\times\alpha\lambda^3+96\cos(\lambda)e^{-\lambda}\alpha^2\lambda^4+16e^{\lambda}\cos(\lambda)\lambda^5\mu-16e^{-\lambda}\cos(\lambda)\lambda^5\mu-12e^{\lambda}\cos(\lambda)\alpha^3\lambda$$
$$-16e^{\lambda}\alpha\lambda^3\sin(\lambda)+12e^{-\lambda}\cos(\lambda)\alpha^3\lambda-16e^{-\lambda}\sin(\lambda)\alpha\lambda^3-48e^{-\lambda}\alpha\lambda^5\mu\sin(\lambda)+32\alpha$$
$$\times\lambda^4\mu+16e^{\lambda}\cos(\lambda)\lambda^4+3e^{\lambda}\cos(\lambda)\alpha^4+16e^{-\lambda}\cos(\lambda)\lambda^4+3e^{-\lambda}\alpha^4\cos(\lambda)-48$$
$$\times\sin(\lambda)e^{\lambda}\alpha^2\lambda^3+12\sin(\lambda)e^{\lambda}\alpha^4\lambda-48\sin(\lambda)e^{\lambda}\alpha^3\lambda^3-48\sin(\lambda)e^{-\lambda}\alpha^3\lambda^3-16\sin(\lambda)$$
$$\times e^{\lambda}\alpha^4\lambda^3-16\sin(\lambda)e^{-\lambda}\alpha^4\lambda^3-48e^{\lambda}\alpha\lambda^5\mu\sin(\lambda)-48\cos(\lambda)e^{-\lambda}\alpha\lambda^5\mu-32\cos(\lambda)$$
$$\times e^{-\lambda}\alpha^2\lambda^4\mu-32e^{\lambda}\alpha^2\mu\lambda^4\cos(\lambda)-48\cos(\lambda)e^{-\lambda}\alpha^2\lambda^5\mu-16\cos(\lambda)e^{-\lambda}\alpha^3\lambda^4\mu$$
$$+48e^{\lambda}\alpha^2\lambda^5\mu\cos(\lambda)-16\cos(\lambda)e^{\lambda}\alpha^3\lambda^4\mu-48\sin(\lambda)e^{-\lambda}\alpha^2\lambda^5\mu-16e^{-\lambda}\alpha\lambda^4\mu$$
$$\times\cos(\lambda)-16e^{\lambda}\cos(\lambda)\alpha\lambda^4\mu-16\sin(\lambda)e^{-\lambda}\alpha^3\lambda^5\mu-16e^{\lambda}\alpha^3\lambda^5\mu\sin(\lambda)$$
$$\left.-48\sin(\lambda)e^{\lambda}\alpha^2\lambda^5\mu-16\cos(\lambda)e^{-\lambda}\alpha^3\lambda^5\mu\right)=0 \quad (3.7)$$

Finally, for given λ and σ, the mode shape can be obtained from $w(x)=\frac{v(x)}{\sigma(x)}$, where, $v(x)$ is given by Eqn. (2.15).

- Beams with quartic variation in width

For a taperd cantilever beam with nonlinearly tapered width $b(x)=b_0(1+\alpha x)^4$, the area moment of inertia and area can be written as $I(x)=I_0(1+\alpha x)^4$ and $A(x)=A_0(1+\alpha x)^4$, respectively. The corresponding expression of σ can be obtained from Eqn. (2.14) as $\sigma(x)=(1+\alpha x)^2$, thus, $A(x)=A_0\sigma(x)^2$ and $I(x)=I_0\sigma(x)^2$. The frequency parameter λ can be found

from the frequency equation

$$\begin{aligned}
&\frac{2\lambda^2}{(1+\alpha)^5}\left(2\alpha^5\lambda^4+10\alpha\lambda^4+10\alpha^4\lambda^4+20\alpha^3\lambda^4+20\alpha^2\lambda^4+24\alpha^5+2\lambda^4-12\cos(\lambda)e^{-\lambda}\alpha^5\right.\\
&-12\cos(\lambda)e^{-\lambda}\alpha^5-24\sin(\lambda)e^{-\lambda}\alpha^4\lambda+36e^{-\lambda}\alpha^3\lambda^2\sin(\lambda)-16\sin(\lambda)e^{-\lambda}\alpha^2\lambda^3-24\sin(\lambda)\\
&\times e^{-\lambda}\alpha^4\lambda-36\sin(\lambda)e^{-\lambda}\alpha^3\lambda^2-16\sin(\lambda)e^{-\lambda}\alpha^2\lambda^3+24\cos(\lambda)e^{-\lambda}\alpha^4\lambda-16\cos(\lambda)e^{-\lambda}\\
&\times\alpha^2\lambda^3+5\cos(\lambda)e^{-\lambda}\alpha\lambda^4-24\cos(\lambda)e^{-\lambda}\alpha^4\lambda+16\cos(\lambda)e^{-\lambda}\alpha^2\lambda^3+5\cos(\lambda)e^{-\lambda}\alpha\lambda^4\\
&-4\cos(\lambda)e^{-\lambda}\alpha^5\lambda^3+5\cos(\lambda)e^{-\lambda}\alpha^4\lambda^4+4\cos(\lambda)e^{-\lambda}\alpha^5\lambda^3+5\cos(\lambda)e^{-\lambda}\alpha^4\lambda^4+12\\
&\times\sin(\lambda)e^{-\lambda}\alpha^5\lambda^2-16\sin(\lambda)e^{-\lambda}\alpha^4\lambda^3-12\sin(\lambda)e^{-\lambda}\alpha^5\lambda^2-16\sin(\lambda)e^{-\lambda}\alpha^4\lambda^3-16\\
&\times\cos(\lambda)e^{-\lambda}\alpha^4\lambda^3+10\cos(\lambda)e^{-\lambda}\alpha^3\lambda^4+16\cos(\lambda)e^{-\lambda}\alpha^4\lambda^3+10\cos(\lambda)e^{-\lambda}\alpha^3\lambda^4-12\\
&\times\sin(\lambda)e^{-\lambda}\alpha^5\lambda+36\alpha^4\lambda^2e^{-\lambda}\sin(\lambda)-24\sin(\lambda)e^{-\lambda}\alpha^3\lambda^3-12\sin(\lambda)e^{-\lambda}\alpha^5\lambda-36\\
&\times\sin(\lambda)\alpha^4\lambda^2e^{-\lambda}-24\sin(\lambda)e^{-\lambda}\alpha^3\lambda^3+12\cos(\lambda)e^{-\lambda}\alpha^5\lambda-24\cos(\lambda)e^{-\lambda}\alpha^3\lambda^3+10\\
&\times\cos(\lambda)e^{-\lambda}\alpha^2\lambda^4-12\cos(\lambda)e^{-\lambda}\alpha^5\lambda+24\cos(\lambda)e^{-\lambda}\alpha^3\lambda^3+10e^{-\lambda}\cos(\lambda)\alpha^2\lambda^4-12\\
&\times e^{-\lambda}\sin(\lambda)\alpha^3\lambda+4e^{-\lambda}\cos(\lambda)\alpha\lambda^3-12e^{-\lambda}\sin(\lambda)\alpha^3\lambda+\cos(\lambda)e^{-\lambda}\alpha^5\lambda^4+\cos(\lambda)\\
&\times e^{-\lambda}\alpha^5\lambda^4-4\sin(\lambda)e^{-\lambda}\alpha^5\lambda^3-4\sin(\lambda)e^{-\lambda}\alpha^5\lambda^3-e^{-\lambda}\sin(\lambda)\lambda^5\mu-e^{-\lambda}\sin(\lambda)\lambda^5\mu\\
&-4e^{-\lambda}\cos(\lambda)\alpha\lambda^3-12e^{-\lambda}\cos(\lambda)\alpha^4+e^{-\lambda}\cos(\lambda)\lambda^4-12e^{-\lambda}\cos(\lambda)\alpha^4+e^{-\lambda}\cos(\lambda)\lambda^4\\
&+\cos(\lambda)e^{-\lambda}\alpha\lambda^5\mu-\sin(\lambda)e^{-\lambda}\alpha\lambda^5\mu-\sin(\lambda)e^{-\lambda}\alpha\lambda^5\mu+24\alpha^4-\cos(\lambda)e^{-\lambda}\alpha\lambda^5\mu\\
&+e^{-\lambda}\cos(\lambda)\lambda^5\mu-e^{-\lambda}\lambda^5\mu\cos(\lambda)+12e^{-\lambda}\cos(\lambda)\alpha^3\lambda+12e^{-\lambda}\sin(\lambda)\alpha^2\lambda^2-4e^{-\lambda}\\
&\times\sin(\lambda)\alpha\lambda^3-12e^{-\lambda}\cos(\lambda)\alpha^3\lambda-12e^{-\lambda}\alpha^2\sin(\lambda)\lambda^2-4e^{-\lambda}\sin(\lambda)\alpha\lambda^3-4e^{-\lambda}\cos(\lambda)\\
&\left.\times\alpha\lambda^4\mu-4e^{-\lambda}\cos(\lambda)\alpha\lambda^4\mu+8\alpha\lambda^4\mu\right)=0
\end{aligned}\tag{3.8}$$

Like linearly tapered beam, for given λ and σ, the mode shape can be obtained from $w(x) = \frac{v(x)}{\sigma(x)}$, where, $v(x)$ is given by Eqn. (2.15).

3.3 Analytical modeling: Nonlinear response

In this section we develop an analytical model to determine the nonlinear frequency response curve for different beams. The method of multiple scales is used to solve the resulting nonlinear equation.

3.3.1 Modal dynamic equation

After obtaining the mode shapes corresponding to different tapered beams, we obtain the modal dynamic equation from Eqn. (3.3) to analyse the tapering effect on the nonlinear frequency response. To obtain the equation, we approximate the transverse deflection $w(x,t)$ by a single mode as $w(x,t) = \phi(x)\eta(t)$, where $\phi(x)$ are the linear undamped mode shape and $\eta(t)$ time dependent variable. After substituting assumed solution, w, in Eqn. (3.3) and then applying the Gelarkin method, we get the following form of generalized modal dynamic equation

$$\ddot{\eta}+S_1\eta+S_2\eta^3+S_3\eta^2\ddot{\eta}+S_4\eta\dot{\eta}^2+S_5\dot{\eta}+S_6\sin(\Omega t)=0, \tag{3.9}$$

where, $S_1,\ S_2,\ S_3,\ S_4,\ S_5,\ S_6$ are the constants given by

$$
\begin{aligned}
S_0 &= \textstyle\int_0^1 (1+f_2(x))\phi(x)^2 dx \\
S_1 &= \tfrac{1}{S_0}\textstyle\int_0^1 \phi(x)\Big(f_1(x)^{''}\phi(x)^{''} + 2f_1(x)^{'}\phi(x)^{'''} + (1+f_1(x))\phi(x)^{''''}\Big)dx \\
S_2 &= \tfrac{1}{S_0}\textstyle\int_0^1 \Big(\phi(x)\phi(x)^{'}\big(f_1(x)^{''}\phi(x)^{''}\phi(x)^{'} + 2f_1(x)^{'}\phi(x)^{'''}\phi(x)^{'} \\
&\quad + 2f_1(x)^{'}(\phi(x)^{''})^2 + (1+f_1(x))\phi(x)^{''''}\phi(x)^{'} \\
&\quad + (3+3f_1(x))\phi(x)^{'''}\phi(x)^{''}\big) - (1+f_1(x)(\phi(x)^{''})^3\phi(x)\Big)dx \\
S_3 &= \tfrac{1}{S_0}\textstyle\int_0^1 (1+f_2(x))\phi(x)\phi(x)^{'}\int_0^x(\phi(x)^{'})^2 dx \\
S_4 &= \tfrac{1}{S_0}\textstyle\int_0^1 (1+f_2(x))\phi(x)\phi(x)^{'}\int_0^x(\phi(x)^{'})^2 dx \\
S_5 &= \tfrac{1}{S_0}\textstyle\int_0^1 \frac{\omega}{Q_f}\phi(x)^2 dx \\
S_6 &= -\tfrac{1}{S_0}\textstyle\int_0^1 \frac{L^3}{EI_0}\phi(x)dx.
\end{aligned}
$$

The above coefficients changes with the tip mass quantity, μ and the non-uniformity of the cantilever beam which is captured by $f_1(x) = \frac{E\tilde{I}(x)}{EI_0}$ and $f_2(x) = \frac{\rho\tilde{A}(x)}{\rho A_0}$. The values of these coefficients are tabulated in Appendix for different tapered beam under given tip mass.

3.3.2 Modulation equation using MMS

In this section, we apply the method of multiple scales [62] to do the nonlinear dynamic analysis of the non-uniform cantilever beam with tip mass. To do the analysis, we first rescale the nonlinear terms in nonlinear modal equation given by Eqn. (3.3) with small quantity ϵ. The resulting dynamic equation with weak nonlinearity can be written as

$$\ddot{\eta} + S_1\eta + \epsilon S_2\eta^3 + +\epsilon S_3\eta^2\ddot{\eta} + \epsilon S_4\eta\dot{\eta}^2 + \epsilon S_5\dot{\eta} + \epsilon S_6\sin(\Omega t) = 0. \tag{3.10}$$

To obtain the modulation equation, we approximate the solution using multiple time scales $T_0 = t$ and $T_1 = \epsilon t$ as $\eta = \eta_1(T_0,T_1) + \epsilon^1\eta_2(T_0,T_1)$, where, $\ddot{\eta} = \Big(D_0^2 + 2\epsilon D_0D_1\Big)\eta;\quad \dot{\eta} = \Big(D_0 + \epsilon D_1\Big)\eta$. Substituting the approximate solution in the governing equation given by Eqn. (3.9) and comparing the coefficient of ϵ^0 and ϵ^1, we get the following two equations

$$\mathcal{O}(\epsilon^0): \qquad D_0^2\eta_1 + \omega^2\eta_1 = 0, \tag{3.11}$$

$$
\begin{aligned}
\mathcal{O}(\epsilon^1): D_0^2\eta_2 + \omega^2\eta_2 = -\Big(&2D_0D_1\eta_1 + S_2\eta^3 + S_3\eta^2(D_0^2\eta) \\
&+S_4\eta_1(D_0\eta_1)^2 + S_5D_0\eta + S_6\sin(\Omega t)\Big),
\end{aligned} \tag{3.12}
$$

where, $D_i^j = \frac{\partial^j}{\partial T_i^j}$, $\omega^2 = S_1$. Assuming the solution of Eqn. (3.11) of the form

$$\eta_1 = A(T_1)e^{(\iota\omega T_0)} + \overline{A}(T_1)e^{(-\iota\omega T_0)} \tag{3.13}$$

and then substituting it in Eqn. (3.12) with $\Omega = \omega + \epsilon\sigma$, where, σ is the detuning parameter, we get

$$\begin{aligned} D_0^2\eta_2 + \omega^2\eta_2 = &\Big(S_3 A(T_1)^3\omega^2 + S_4 A(T_1)^3\omega^2 - S_2 A(T_1)^3\Big)\Big(e^{(i\omega T_0)}\Big)^3 \\ &+\Big(- 2i\dot{A}(T_1)\omega - 3S_3 A(T_1)^2\overline{A}(T_1) + 3S_3 A(T_1)^2\overline{A}(T_1)\omega^2 \\ &-S_4 A(T_1)^2\overline{A}(T_1)\omega^2 - iS_5 A(T_1)\omega + \frac{1}{2}iS_6 e^{i\sigma T_1}\Big)e^{i\omega T_0} + cc, \end{aligned} \tag{3.14}$$

where, *cc* represents the complex conjugate part of the equation. To get the converged solution, we eliminate the secular terms from Eqn. (3.14) which gives complex modulation equation as

$$\begin{aligned} &\Big(- 2i\dot{A}(T_1)\omega - 3S_3 A(T_1)^2\overline{A}(T_1) + 3S_3 A(T_1)^2\overline{A}(T_1)\omega^2 \\ &-S_4 A(T_1)^2\overline{A}(T_1)\omega^2 - iS_5 A(T_1)\omega + \frac{1}{2}iS_6 e^{i\sigma T_1}\Big) = 0. \end{aligned} \tag{3.15}$$

To obtain the real and autonomous form of Eqn. (3.15), we substitute $A(T_1) = \frac{1}{2}a(T_1)e^{i\omega\phi(T_1)}$ in Eqn. (3.15) and then equate the real and imaginary parts, separately. Taking $\theta = \sigma T_1 - \phi$ and $\dot{\theta} = \frac{d\theta}{dT_1}$, we get the following modulation equations

$$a\dot{\theta} = \sigma + \frac{3}{8}\omega S_3 a^3 - \frac{1}{8}\omega S_4 a^3 - \frac{3}{8\omega}S_2 a^3 - \frac{1}{2\omega}S_6\sin(\theta) \tag{3.16}$$

$$\dot{a} = -\frac{1}{2}S_5 a + \frac{1}{2\omega}S_6\cos(\theta). \tag{3.17}$$

The above equations can be solved to obtain nonlinear response using continuation software, MATCONT.

3.4 Results and discussion

In this section, we present the effect of mass sensitivity on the linear and nonlinear frequency response of uniform as well as non-uniform cantilever beam. We first discuss about the changes associated with linear frequency due to tapering at different tip mass and then the corresponding nonlinear effect. It is important to note that the linear and nonlinear analysis are presented in non-dimensional quantities. Hence, the results can be generalized for cantilever beam with any real dimensions.

3.4.1 Mass effect on linear frequency

In this section, we discuss the effect of added mass and the non-uniformity parameter on the linear frequency of different types of cantilever beams. Utilizing the mode shapes obtained in the previous section for various non-uniform cantilever beams, we determine the eigenvalues by solving the corresponding frequency equation. Additionally, we also obtain the modal frequencies for different beams by finite element analysis using ABAQUS. Subsequently, we present the first three linear frequencies of various beams and compared them with the existing references. Finally, we analyze the mass sensitivity of the tapered beam with respect to the uniform beam. Following the same procedure as explained in Chapter 2, modal frequencies for different beams with tip mass at the end are obtained using ABAQUS. These frequencies are compared with the presented model and is found to be in excellent agreement. In the subsequent sections, the frequencies with different tip masses at the end

are tabulated and compared.

1. Uniform beam For uniform beam, the mode shape and the associated boundary conditions are given by Eqns. (3.5) and (3.4), respectively. We then solve the transcedental equation given by Eqn. (3.6) for various non-dimensional tip mass, μ, to determine the non-dimensional linear frequency of the beam. The first, second and third modes are mentioned in Table 3.1. We also compare the fundamental frequency for various tip mass with existing results obtained by Kim *et al* [50]. The results are found to be in good agreement. Thus, the approach adopted in this analysis is validated and can be extended to compute frequencies of non-uniform beams with different tapering.

Table 3.1: The nondimensional fundamental frequency of uniform beam with added mass.

μ	Mode	Present	Kim *et al.* [7]	ABAQUS
0.0	1	3.5160	3.516	3.5292
	2	22.0345	-	22.0637
	3	61.6972	-	61.8717
0.1	1	2.9678	2.968	-
	2	19.3558	-	-
	3	55.5183	-	-
0.2	1	2.6127	2.613	2.6189
	2	18.2078	-	18.081
	3	53.5586	-	51.7742
0.3	1	2.3597	2.356	-
	2	17.5756	-	-
	3	52.6156	-	-
0.4	1	2.1679	2.168	-
	2	17.1763	-	-
	3	52.0632	-	-

2. Beams with linear variation in width

   In this case, we consider two types of linearly tapered beams in our analysis. First, we consider the linearly diverging beam, where, α is positive, and the other is linearly converging beam, where, α is negative. The schematic diagram of such geometry can be seen in Fig. **??**. For a linearly tapered beam, solving the transcendental equation given by Eqn. (3.7), we obtain the non-dimensional linear frequency and the corresponding mode shape for various tip mass parameter, μ, as well as the tapered parameter α. Tables 3.2 list the first three non-dimensional frequencies of a linearly tapered beam for different α without ($\mu = 0.0$) and with ($\mu = 0.2$) added tip mass. Tables 3.3, 3.4 lists the first three frequencies for $\alpha = \pm 0.2 and \pm 0.4$ for different μ. The computed frequencies are also compared with the frequency obtained by Mabie *et. al* [54], who obtained the results using numerical integration without finding any exact mode shape and with finite element simulations using ABAQUS. Figure 3.2 presents a comparative graph for linear and quartic beams with tip masses obtained using the presented method and ABAQUS.

   Figure 3.3(a) and (b) show the variation of the natural frequency with the tapered parameter, α, for different μ. For a diverging beam, the frequency decreases with increasing tapering, however, for a converging beam the frequency increases upto a certain α and then it starts de-

Table 3.2: The nondimensional frequency for beam with linear variation in width. (Left) When there is no tip mass i.e. $\mu = 0$. (Right) When tip mass $\mu = 0.2$.

α	Mode	Present Model	ABAQUS	Ref. [10]	α	Mode	Present Model	ABAQUS	Ref. [10]
	1	3.516	3.529	3.516		1	2.613	2.619	2.613
0	2	22.035	22.063	22.035	0	2	18.208	18.081	18.208
	3	61.697	61.872	61.700		3	53.559	51.7749	53.550
	1	3.628	3.642	-		1	2.641	2.647	-
-0.1	2	22.258	22.230	-	-0.1	2	18.213	18.094	-
	3	61.915	62.082	-		3	53.451	51.999	-
	1	3.747	3.771	3.717		1	2.662	2.677	2.720
-0.2	2	22.523	22.516	22.415	-0.2	2	18.228	18.102	18.348
	3	62.180	62.280	62.060		3	53.354	52.146	53.580
	1	3.865	3.922	-		1	2.667	2.708	-
-0.3	2	22.835	22.791	-	-0.3	2	18.260	18.102	-
	3	62.504	62.536	-		3	53.275	52.228	-
	1	3.954	4.098	3.892		1	2.633	2.740	2.810
-0.4	2	23.207	23.105	22.743	-0.4	2	18.314	18.095	18.451
	3	62.910	62.811	62.390		3	53.227	52.255	53.580
	1	3.940	4.312	-		1	2.506	2.772	-
-0.5	2	23.645	23.487	-	-0.5	2	18.402	18.077	-
	3	63.429	63.172	-		3	53.231	52.232	-
	1	3.5400	4.578	4.049		1	2.114	2.805	2.886
-0.6	2	24.129	23.967	23.030	-0.6	2	18.542	18.046	18.530
	3	64.101	63.653	62.680		3	53.329	52.158	53.570

creasing. For a diverging beam, the shift in the natural frequency for a cantilever beam without added mass ($\mu = 0$) and with added mass gradually reduces with increasing α. However for a converging beam, this shift increases with α, even though, the frequency decreases after certain α. On comparing the non-dimensional frequency shift, Δf, subjected to non-dimensional tip mass, μ, we obtain the non-dimensional mass sensitivity $S = \Delta f/\mu$. On comparing the variation of mass sensitivity, S, for linearly converging and diverging tapered beam as shown in Fig. (3.4)(a), we found that S increase for converging beam, but it decreases for diverging beam. Hence, a converging beam is a suitable design for an effective mass sensor.

3. Beams with quartic variation in width

   To check the suitability of non-linearly varying non-uniform beam, we take quartic polynomial for the variation of width. Like linear case, we take both, the diverging beam (positive α) as well as converging beams (negative α). To find the non-dimensional frequency and the mode shape, we solve the transcendental equation given by Eqn. (3.8) corresponding to different α and non-dimensional tip mass, μ. Tables 3.5 mentions the first three non-dimensional frequencies for different α at $\mu = 0.0$ and $\mu = 0.2$. Table 3.6 and 3.7 lists the first three frequencies for $\alpha = \pm 0.2$ and $\alpha = \pm 0.4$ at different μ. Figures 3.3(c) and (d) show the variation of the natural frequency with non-uniform parameter (α) for different μ. Additionally, Fig. 3.5 presents a comparative graph for linear and quartic beams with tip masses obtained using the presented method and ABAQUS.

   For a diverging beam, the frequency decreases with an increase in α, while for a converging

Table 3.3: The frequency of converging beam ($\alpha = -0.2$ and $\alpha = -0.4$) with linear variation in width.

μ	Mode	Present	Ref. [10]	μ	Mode	Present	Ref. [10]
0.0	1	3.7475	3.7168	0.0	1	3.9542	3.8923
	2	22.5225	22.415		2	23.2068	22.743
	3	62.1796	62.06		3	62.9099	62.39
0.2	1	2.6621	2.7202	0.2	1	2.6329	2.8100
	2	18.2282	18.348		2	18.3137	18.451
	3	53.3539	53.58		3	53.2266	53.58
0.4	1	2.1729	2.2440	0.4	1	2.1060	2.3061
	2	17.2344	17.312		2	17.3891	17.414
	3	52.0000	52.13		3	52.0544	52.17
0.6	1	1.8809	1.9527	0.6	1	1.8052	2.0017
	2	16.7964	16.844		2	17.0016	16.951
	3	51.4600	51.54		3	51.6045	51.60
0.8	1	1.6816	1.7517	0.8	1	1.6047	1.7924
	2	16.5500	16.576		2	16.7888	16.690
	3	51.1701	51.21		3	51.3669	51.29

Table 3.4: The frequency of diverging beam ($\alpha = 0.2$ and $\alpha = 0.4$) with linear variation in width.

$\alpha = 0.2$	μ	Mode	Freq.	$\alpha = 0.4$	μ	Mode	Freq.
	0.0	1	3.3205		0.0	1	3.1626
		2	21.6746			2	21.3998
		3	61.3568			3	61.1044
	0.2	1	2.5523		0.2	1	2.4963
		2	18.2185			2	18.2446
		3	18.2185			3	54.0184
	0.4	1	2.1471		0.4	1	2.1248
		2	17.1679			2	17.1866
		3	52.1812			3	52.3258
	0.6	1	1.8881		0.6	1	1.8809
		2	16.6637			2	16.6605
		3	51.4948			3	51.5796
	0.8	1	1.7046		0.8	1	1.7051
		2	16.3680			2	16.3461
		3	51.1148			3	51.1605

Table 3.5: The nondimensional frequency for beam with quartic variation in width. (Left) When there is no tip mass i.e. $\mu = 0$. (Right) When tip mass $\mu = 0.2$.

α	Mode	Present Model	ABAQUS	α	Mode	Present Model	ABAQUS
	1	3.516	3.529		1	2.613	2.619
0	2	22.0345	22.064	0	2	18.208	18.081
	3	61.697	61.872		3	53.559	51.774
	1	3.994	3.902		1	2.717	2.714
-0.1	2	22.925	22.374	-0.1	2	18.200	18.094
	3	62.569	61.147		3	53.160	52.072
	1	4.587	4.466		1	2.780	2.768
-0.2	2	23.960	23.330	-0.2	2	18.197	18.091
	3	63.620	62.006		3	52.898	52.204
	1	5.336	5.178		1	2.787	2.767
-0.3	2	25.194	24.468	-0.3	2	18.242	18.112
	3	64.914	63.088		3	52.835	52.247
	1	6.298	6.240		1	2.726	2.699
-0.4	2	26.709	26.504	-0.4	2	18.382	18.214
	3	66.554	66.081		3	53.022	52.394
	1	7.558	7.466		1	2.591	2.560
-0.5	2	28.651	28.364	-0.5	2	18.655	18.439
	3	68.715	68.066		3	53.491	52.748
	1	9.235	9.096		1	2.380	2.349
-0.6	2	31.282	30.901	-0.6	2	19.084	18.808
	3	71.728	70.902		3	54.271	53.338

beam it increases with an increase in the magnitude of α. For a diverging beam, the shift in the frequency for a cantilever beam without added mass ($\mu = 0$) and with added mass gradually reduces with increasing non-uniform parameter. However, for a converging beam, this shift increases sharply with the nonuniform parameter. Consequently, we found that the non-dimensional mass sensitivity, S, drastically increases by an order of magnitude higher as compared to that for uniform beam when α varies from 0 to 0.6 as shown in Fig. (3.4)(a). Moreover, we have also found from Fig. (3.4)(b) that S increases by around 5 times, if the non-uniform beam with quartic tapering at tapering ratio $\alpha = 0.6$ operates in its 5^{th} mode. This makes a converging beam with nonlinear tapering, here, quartic variation, a better and suitable design for an effective mass sensor as compared to beam with linearly tapered width. Now, we investigate the influence of tapering parameter on the non-linear response under different tip masses.

3.4.2 Mass effect on non-linear frequency

In this section, we present the effect the non-uniform parameter and the tip mass on the non-linear frequency response of various types of cantilever beams. To do the nonlinear analysis, we first validate the solution of modulation equation with the numerical solution of the parent equation given by Eqn. (3.10) in the following section.

Table 3.6: The frequency of converging beam ($\alpha = -0.2$ and $\alpha = -0.4$) with quartic variation in width.

$\alpha = -0.2$	μ	Mode	Frequency	$\alpha = -0.4$	μ	Mode	Frequency
	0.0	1	4.5877		0.0	1	6.2980
		2	23.9601			2	26.7090
		3	63.6203			3	66.5539
	0.2	1	2.7796		0.2	1	2.7257
		2	18.1968			2	18.3821
		3	52.8975			3	53.0215
	0.4	1	2.1695		0.4	1	2.018
		2	17.3885			2	17.9269
		3	51.9706			3	52.6062
	0.6	1	1.8391		0.6	1	1.6746
		2	17.0694			2	17.7655
		3	51.6293			3	52.4631
	0.8	1	1.6245		0.8	1	1.4623
		2	16.8987			2	17.6830
		3	51.4520			3	52.3906

Table 3.7: The frequency of diverging beam ($\alpha = 0.2$ and $\alpha = 0.4$) with quartic variation in width.

$\alpha = 0.2$	μ	Mode	Frequency	$\alpha = 0.4$	μ	Mode	Frequency
	0.0	1	2.7993		0.0	1	2.2943
		2	20.5644			2	19.3823
		3	60.3289			3	59.3020
	0.2	1	2.3414		0.2	1	2.0539
		2	18.1209			2	17.8439
		3	54.4955			3	55.2865
	0.4	1	2.0517		0.4	1	1.8754
		2	17.0953			2	16.9797
		3	52.6543			3	53.4432
	0.6	1	1.8478		0.6	1	1.7363
		2	16.5345			2	16.4284
		3	51.7674			3	52.4000
	0.8	1	1.6945		0.8	1	1.6241
		2	16.1814			2	16.0465
		3	51.2473			3	51.7317

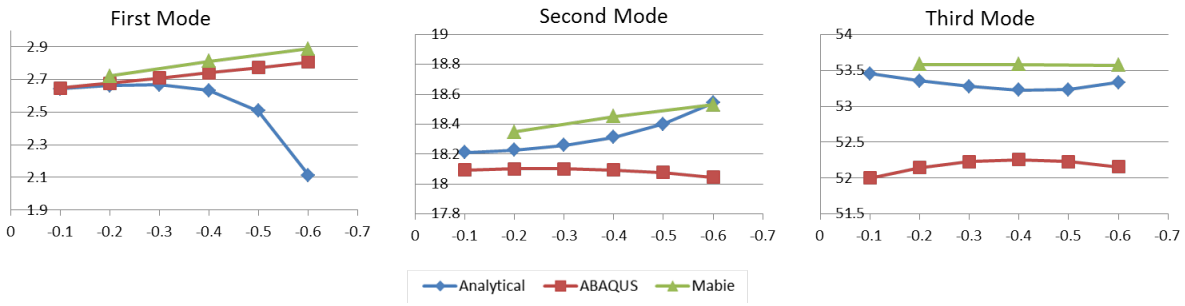

Figure 3.2: Comparison of first three frequencies for beams ($\mu = 0.2$)with linear variation in width for different α obtained from the presented analytical mode, ABAQUS and that of Mabie [21].

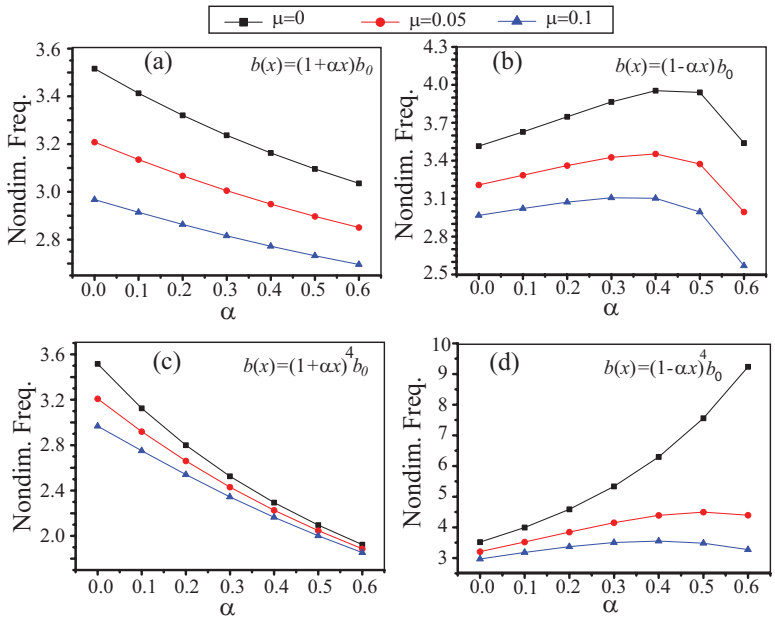

Figure 3.3: The variation of nondimensional fundamental frequency with the tapering parameter α and tip mass μ for (a) diverging beam with linear tapering, (b) converging beam with linear tapering, (c) diverging beam with quartic tapering, and (d) converging beam with quartic tapering.

Numerical validation

In order to ensure that the approximate solution can be used effectively to study the various nonlinear effects, we first validate the results obtained from MMS with the numerical results. We solve the evolution equation given by Eqns. (3.16) and (3.17) in MATCONT for the values of coefficients as given in Table 1 in Appendix B. Subsequently, we solve the governing equation Eqn. (3.9) using the Runge-Kutta method to obtain the nonlinear response. Figure 3.6 shows the comparative results for uniform beam, converging beam with linear variation and converging beam with quartic variation in width. The results show that the modulation equation can be used to do further analysis of tapered beam.

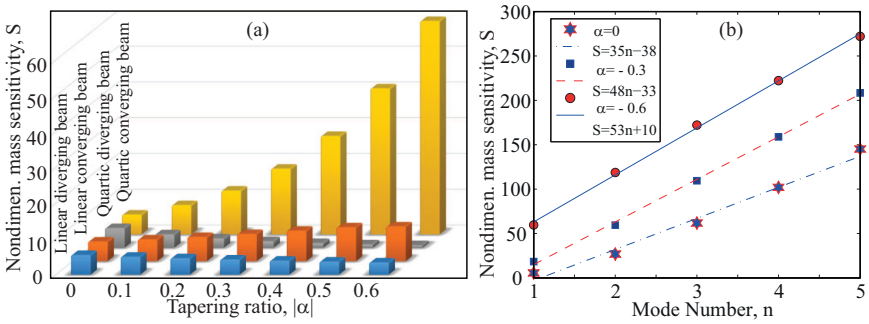

Figure 3.4: (a) Variation of non-dimensional mass sensitivity with tapering ratio for different types of tapering; (b) Variation of non-dimensional mass sensitivity versus mode number for uniform, $\alpha = 0$, and non-uniform beam with quartic converging cross-section where, $\alpha = -0.3$ and $\alpha = -0.6$.

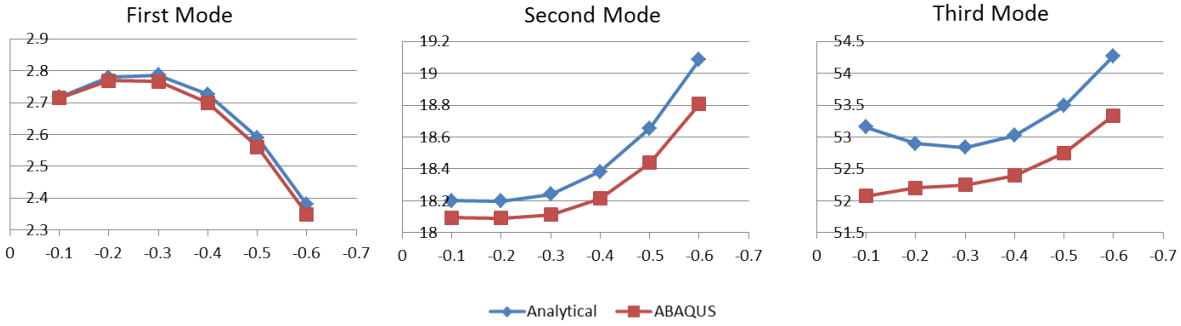

Figure 3.5: Comparison of first three frequencies for beams ($\mu = 0.2$) with quartic variation in width for different α obtained from the presented analytical mode and ABAQUS

Uniform beam

In this section, we plot the non-linear frequency response for a uniform beam as shown in Fig. 3.7. Figure 3.7(a) shows the response for various forcing. As the forcing is increased, the amplitude increases and the system becomes more of softening type. Figure 3.7(b) shows the frequency response for $\mu = 0,\ 0.05,\ 0.1$. It shows that the response amplitude increases with an increase in added mass. At the same time, the system tends to be of softening type as the mass is increased which leads to shift in the frequency corresponding to the peak value. Hence, we can define the non-dimensional mass sensitivity in this case as the ratio of frequency shift corresponding to the peak to the non-dimensional tip mass. Now, we discuss the tapering effect of non-uniform beam in the following section.

Beams with linear variation in width

Figure 3.8 show the effect of added mass on the nonlinear response of a linearly diverging beam under the external force $F = 0.01$. Figures 3.8(a) and (b) show the graphs for three values of $\mu = 0,\ 0.05$ and 0.1 when $\alpha = 0.1$ and 0.3, respectively. The analysis of graphs show that the peak amplitude as well as its corresponding frequency shift increases as the non-dimensional tip mass, μ, increases for a given non-uniform factor α. For a given change in tip mass of 0.1, we have found that the change in non-dimensional frequency Δf increases linearly with non-uniform factor α as $\Delta f = 0.04|\alpha| + 0.025$.

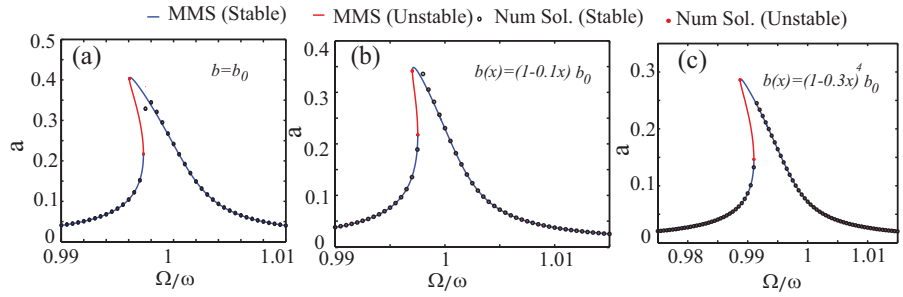

Figure 3.6: Numerical and approximate solution for (a) uniform beam, (b) converging beam with linear tapering, and (c) converging beam with quartic tapering.

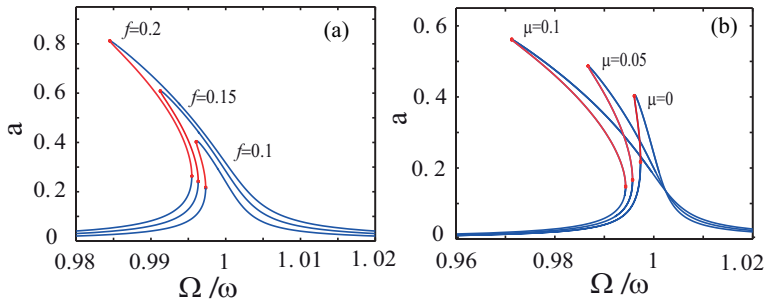

Figure 3.7: Non-linear frequency response of a uniform beam with varying (a) forcing and (b) added mass.

It gives a change of about 0.02 when the non-uniform factor, α, changes from 0.1 to 0.6 as shown in Figure 3.8(c). The relative change in amplitude is found to be very small. Moreover, an analysis of the coefficients of non-linear equation in Appendix B shows that the inertial nonlinearity does not change significantly with tip mass but geometrical nonlinearity reduces remarkably. At the same time, with increase in tapering parameter, the inertial nonlinearity decreases marginally and the geometrical nonlinearity decreases significantly. Consequently, the increase in taper parameter leads to more nonlinear softening of the system.

Similarly, Figures 3.9(a) and (b) show the effect of mass on the nonlinear response of converging beam with negative α, i.e., -0.1 and -0.3, under the external force $F = 0.01$, for $\alpha = 0.1$ and 0.3. From the nonlinear response curve, we see that for a converging beam the change in response amplitude as well as the softening effect are less than those of the diverging beam. Unlike the case with diverging beam, we observed that the change in non-dimensional frequency Δf in this case decreases linearly with increase in non-uniform parameter $|\alpha|$ as $\Delta f = -0.04|\alpha| + 0.027$ as shown in Figure 3.9(c). However, the level of change is found to be around 0.02 which is same as that in diverging beam. Based on the corresponding values of coefficients as mentioned in Table 1, we observed that the inertial nonlinearity depends weakly on the added mass while the geometrical nonlinearity depends strongly on it. Additionally, we found that the inertial nonlinearity increases (marginally) while the geometrical nonlinearity increases significantly with increase in tapering parameter. Consequently, due to increase in nonlinear stiffness, the nonlinear softening effect reduces. Hence, the frequency shift corresponding to the peak amplitude decreases as the non-uniform parameter increases in the

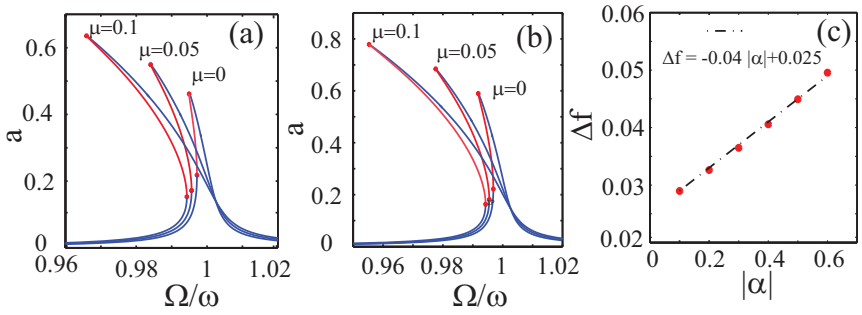

Figure 3.8: Effect of added mass on the nonlinear frequency response of diverging beam with linear variation in width for different taper parameter (a) $\alpha = 0.1$, $F = 0.01$ and (b) $\alpha = 0.3$, $F = 0.01$. (c) Variation of peak frequency shift Δf versus absolute value of α when μ changes from 0 to 0.1.

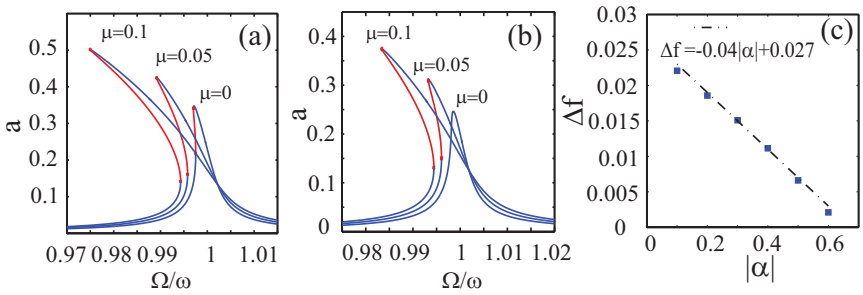

Figure 3.9: Effect of added mass on the nonlinear frequency response of a converging beam with linear variation in width for different taper parameter (a) $\alpha = -0.1$, $F = 0.01$ and (b) $\alpha = -0.3$, $F = 0.01$. Variation of peak frequency shift Δf versus absolute value of α when μ changes from 0 to 0.1.

case of converging beam.

Beams with quartic variation in width

Figures 3.10(a) and (b) show the effect of added mass on the nonlinear response of a diverging beam with quartic polynomial for three values of $\mu = 0$, 0.05 and 0.1 corresponding to the forcing of $F = 0.01$. Like previous cases, for a given tapering, the response amplitude increases marginally with increase in added mass. However, as the taper parameter increases, the shift in non-dimensional frequency Δf corresponding to the response peak increases by a change of 0.6 as α changes from 0.1 to 0.6 when μ changes from 0 to 0.1 as shown in Figure 3.10(c). The variation of Δf versus α is found to be exponential increasing function as $\Delta f = 0.027 \exp(5.25|\alpha|)$. The change in frequency is found to be around 30 times more than that of linearly diverging beam. From Appendix B, it is found that the inertial nonlinearity does not change significantly with tip mass but the geometrical nonlinearity changes significantly as compared to the corresponding nonlinearities in linearly tapered beam. With increase in tapering, the inertial nonlinearity decreases marginally while geometrical nonlinearity decreases significantly. Consequently, it led to the conclusion that increase in taper parameter increases the softening effect of the system as compared to that of linearly tapered beam under the same forcing.

For a converging beam with negative α, Figures 3.11(a) and (b) show the effect of mass on the nonlinear response of beam with $\alpha = -0.3$ and -0.6 under external forcing of $F = 0.1$. As

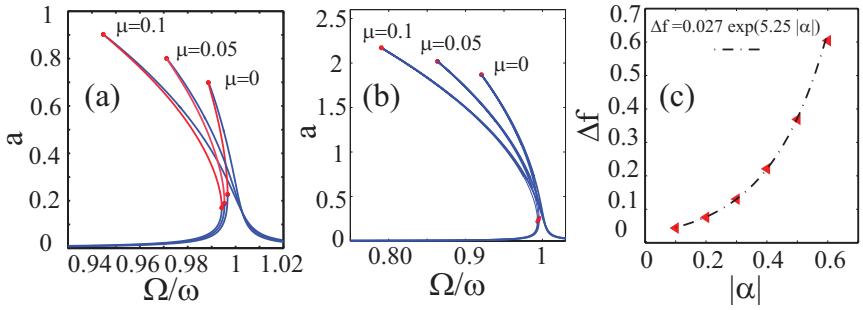

Figure 3.10: Effect of added mass on the nonlinear frequency response of diverging beam with quartic variation in width for different taper parameter (a) $\alpha = 0.1,\ F = 0.01$ and (b) $\alpha = 0.3,\ F = 0.01$. (c) Variation of peak frequency shift Δf versus absolute value of α when μ changes from 0 to 0.1.

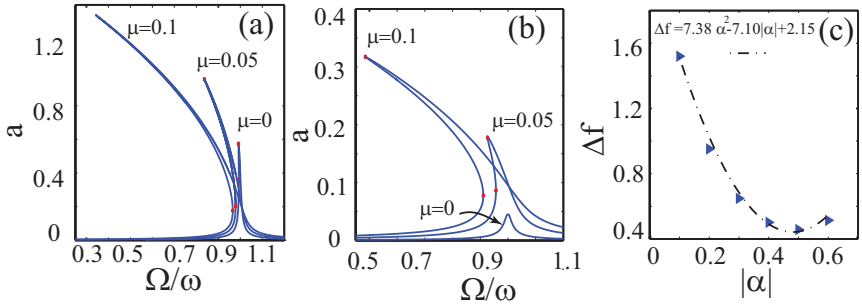

Figure 3.11: Effect of added mass on the nonlinear frequency response of converging beam with quartic variation in width for different taper parameter (a) $\alpha = -0.3,\ F = 0.1$ and (b)$\alpha = -0.6,\ F = 0.1$. (c) Variation of peak frequency shift Δf versus absolute value of α when μ changes from 0 to 0.1.

already stated from the analysis in Chapter 2, the non-dimensional linear frequency increases with increase in non-uniform parameter for a converging beam as shown in Fig.3.3(d). As a result, the non-dimensional damping increases with an increase in α. Consequently, the response amplitude become very low as the damping increases. In order to obtain the nonlinear response, the forcing is increased 10 times for $\alpha = 0.3$ and $\alpha = 0.6$. However, with increased forcing the trend in the peak amplitude for the beams was same as that at low forcing for the corresponding linearly converging beams. From the response curves shown in Figs. 3.11(a) and (b), we see that even at increased forcing the peak response amplitude decreases when α changes from 0.3 to 0.6, when μ changes from 0 to 0.1 as was observed for linearly converging beams. Corresponding to the same change in μ from 0 to 0.1, the non-dimensional frequency shift Δf first decreases as α increases from 0.1 to 0.5 and then starts to increase as α increases beyond 0.6 due to corresponding changes in geometric non-linearity. Consequently, there exist a minimum point at around $\alpha = 0.5$. Thus, by varying the tapering ratio of converging beam with quartic variation in width, the variable mass sensitivity can be obtained.

Finally, we state that we have analyzed the mass sensitivity based on the linear and nonlinear response of uniform and non-uniform cantilever beam with different types of tapering. We have noticed that both linear frequency as well as nonlinear frequency response show higher degree of mass sensitivity for non-uniform converging beam with quartic variation in width at $\alpha = -0.6$. The analysis presented in the chapter can form the basis for future design of non-uniform cantilever

beams in the development of many sensors and actuators.

3.5 Conclusions

In this chapter, we have presented the mass sensitivity of uniform and non-uniform beam with different tapered conditions. To do the analysis, we first derive the nonlinear partial differential equation for non-uniform beam with nonlinear curvature effect. Afterwards, we obtain the exact form of the mode shape for uniform and nonuniform beam with linear and quartic variation width of beam. After obtaining the exact mode shape, we first obtain the linear frequency of different types of beam for different modes. Subsequently using the mode shapes, we derive the nonlinear modal dynamic equation. Finally, we obtain the modulation equation using the method of multiple scale, which is solved using MATCONT. On analysing the influence of tip mass μ as well as tapering parameter, α, on the linear frequency and nonlinear frequency response, we found that the converging tapered beam with quartic variation in width can be used to increase the mass sensitivity remarkably.

Chapter 4

Size-effects on micro-beams

4.1 Introduction

MEMS/NEMS based sensors and actuators widely uses micro/nano beams and plates as the sensing element. The mechanical properties of the beams and plates constitutes the working principles of these sensors and actuators. Owing to the small sizes of these beams, the size-dependent effects greatly influences the dynamic characteristics [72, 73, 74]. As a result, for improved and accurate performance it is vital to capture the size effect associated with these low dimensional beams. The continuum theory fails to capture this size effect on micro structures due to the absence of any material length scale parameter in the governing equation. In order to overcome this, non-classical continuum theories like nonlocal theory [75], modified coupled stress theory (MCST) [76], modified strain gradient elasticity theory (MSGT)[77] etc. have been proposed which contains one or more additional material length scale parameter to capture the size effects. The nonlocal and the modified coupled stress theories incorporate an additional length scale parameter while the modified strain gradient elasticity theory incorporates three additional length scale parameters to capture the size effects. These non-classical models recover the classical model when the additional length scale parameter is set to zero as will be shown in subsequent sections.

Nonlocal elasticity theory based on Eringen and Edelen [75] has been used for vibrational problems. Reddy [91] studied the characteristics of different beams by reformulating the governing equation based on nonlocal theory. Murmu and Pradhan [92] studied vibration response of non-uniform cantilever beams using the nonlocal theory. Janghornan [93] studied the vibration characteristics of tapered nanowires with simply supported as well as clamped boundary conditions on both the ends again using the nonlocal Euler theory. Danesh *et al* [94] studied the small scale effect of tapered nano rods using the nonlocal elasticity theory. Chang [95] and Simsek [96] studied the vibrational characteristics of nonuniform as well as non-homgenous nano rods using the nonlocal elasticity theory. Jang *et al* [97] carried out the static analysis of beams with different end conditions as well as columns, membranes and plates. Kaisy *et al* [98] studied the longitudinal vibrations of non-uniform nano rods.

The modified coupled stress theory has also been used to study the static and dynamic behavior of microbeams. Yang *et al* presented the modified couple stress approach for vibrational analysis [76]. It comprises of an additional internal material length scale parameter. Park *et al* [99] studied

the characteristics of cantilever beams using the MCST. Akgoz and Omar [100] again used the MCST to study the dynamic problems of non-uniform cantilever beams. Ma *et al* [101] used the MCTS to study the vibrational characteristics of Timoshenko beam. Salamat *et al* [102] also used the modified strain gradient theory to analyze functionally graded beams with simply supported end conditions. Lam *et al* proposed the modified strain gradient elasticity theory which uses an additional equation pertaining to equilibrium of moments of couples in addition to the classical equilibrium equation of moments and forces to govern the behavior of higher order stresses [77, 103]. Kong *et al* [104] used the MSGT to study the static and dynamic characteristics of cantilever beams. Their analysis incorporated three additional material length scale parameters to capture the size effect. However, their analysis is limited to cantilever beams. Since, the closed form solution of these equations are difficult to obtain under different boundary conditions, we employ Differential Quadrature Method (DQM) to solve equations based on the above theories.

DQM proposed by Bellman *et al* [78] is an efficient method to solve differential equations using just a few grid points. The pioneering work in the application of DQM was to solve structural problems [79, 80, 81, 82, 83, 84, 85]. However, since then it is being used to solve a variety of problems [86, 87, 88, 89, 90]. Researchers in the past have used DQM to solve vibrational problems associated with different mechanical elements such as beams, plates, rods, shells, tanks, etc. DQM has also been used for vibrational analysis of beams and rods based on nonlocal theory [92, 93, 94, 95, 97, 98]. In this paper, we present the vibrational analysis of beams based on the modified strain gradient elasticity theory using the approach as proposed by Kong *et al* [104]. Their derivation however mis-calculated the coefficient which was later corrected by Akgoz and Civalek [105] and the value of the length scale parameter which was later corrected by Amir [106]. Thus, the analysis based on the modified strain gradient elasticity theory requires re-look through different methods. Additionally, the previous analysis is found to be mainly limited to cantilever beams. In this work, we correct all these anomalies and extend the analysis for clamped and simply supported beams. We use the DQ method with two different techniques for implementing different boundary conditions. We show that the implementation of DQM is simple, accurate and fast. We start with a discussion on DQM, followed by the formulation of governing equation using DQM. Lastly, the first three frequencies for all types of beams based on different theories are compared and the change in frequencies due to the effective capturing of size-dependent effects are discussed.

4.1.1 Differential Quadrature Method (DQM)

The DQM is a numerical method which reduces the partial differential equations into algebraic equations. The central idea behind DQM is to approximate the spatial derivative of a function at a point with weighted linear combination of the functional value at all other points in the domain as shown mathematically in Eqns. (4.1) and (4.2) as

$$\left.\frac{d^n f(x)}{dx^n}\right|_{x=x_i} \approx \sum_{j=1}^{N} C_{ij}^n f(x_j) \qquad i = 1, 2...N \tag{4.1}$$

or,

$$\frac{d^n}{dx^n}\begin{bmatrix} f(x_1) \\ f(x_2) \\ \vdots \\ f(x_{N-1}) \\ f(x_N) \end{bmatrix} \approx [C_{ij}^n] \begin{bmatrix} f(x_1) \\ f(x_2) \\ \vdots \\ f(x_{N-1}) \\ f(x_N) \end{bmatrix} \qquad i,j = 1,2,3 \ldots N \tag{4.2}$$

where, $f(x_i)$ is the functional value at the i^{th} sampling point of the total N points, $[C_{ij}^n]$ is the weighing coefficient matrix of the n^{th} order differential equation. It reduces the PDE into a set of algebraic equations. The number of such algebraic equation depends on the number of sample points taken. Here, domain is discritized into N sampling points using the Chebyshev-Gauss-Lobatto distribution given by

$$X_i = \frac{1}{2}\left[1 - \cos\Big(\frac{i-1}{N-1}\pi\Big)\right], \qquad i = 1,2 \ldots, N. \tag{4.3}$$

The weighing coefficient matrix can now be generated using the sampling distribution as mentioned above using the following relations

$$\begin{aligned} C_{ij}^1 &= \frac{L^1(x_i)}{(x_i - x_j)L^1(x_j)}, \qquad i,j = 1,2,\ldots N, i \neq j, \\ C_{ii}^1 &= -\sum_{j=1,j\neq i}^{N} C_{ij}^1, \qquad i,j = 1,2,\ldots N, i = j, \end{aligned} \tag{4.4}$$

where, L^1 is the first derivative of Lagrange interpolating polynomials at the sampling points given by

$$L^1(x_i) = \prod_{k=1,k\neq i}^{N} \big(x_i - x_k\big), \qquad i = 1,2,\ldots,N. \tag{4.5}$$

The corresponding weighted coefficient matrices for higher order derivatives can be obtained using the relation

$$\begin{aligned} C_{ij}^n &= n\Big(C_{ij}^{n-1}C_{ij}^1 - \frac{C_{ij}^{n-1}}{x_i - x_j}\Big), i,j = 1,2,\ldots,N, i \neq j, n = 2,3,\ldots,N-1, \\ C_{ii}^n &= -\sum_{j=1,j\neq i}^{N} C_{ij}^n, \qquad i,j = 1,2,\ldots N, i = j, n = 2,3,\ldots,N-1. \end{aligned} \tag{4.6}$$

At the same time, the correct implementation of boundary conditions is vital in order to successfully implement DQ method. Different techniques have been proposed to incorporate different boundary conditions. In our analysis we use the δ-technique [77] to solve vibrational problems with clamped-free (CF) boundary conditions and the SBCGE technique [91] for clamped-clamped (CC) and simply supported (SS) boundary conditions. In the subsequent sections, we will discuss the formulation and the implementation of boundary conditions in detail

4.2 Formulation

In this section, we re-write the governing equation of motion and the associated boundary conditions of the Euler-Bernoulli beams with different end conditions based on the strain gradient elasticity theory as done by Kong *et al* [104]. Subsequently, we write the governing equations and the boundary conditions in its equivalent discretized form using DQM. The terms comprising of spatial derivative is replaced with its equivalent weighted coefficient as discussed earlier. We start with the governing equation in the differential form followed by the boundary conditions.

4.2.1 Governing equation based on non-classical theory

The governing equations based on the modified strain gradient theory is derived using the Hamilton's principle. The strain energy based on MSGT can be written as [104, 105]

$$U = \frac{1}{2}\int_0^L [S(w^2)^2 + K(w^3)^2]dx \tag{4.7}$$

and the kinetic energy can be written as

$$T = \frac{1}{2}\int_0^L \rho A(\frac{\partial w}{\partial t})^2 dx, \tag{4.8}$$

where,

$$\begin{aligned} S = EI + 2\mu A l_0^2 + \frac{8}{15}\mu A l_1^2 + \mu A l_2^2, \\ K = I(2\mu l_0^2 + \frac{4}{5}\mu l_1^2), \\ w^n = \frac{\partial^n w}{\partial x^n}, \quad \ddot{w} = \frac{\partial^2 w}{\partial t^2}. \end{aligned} \tag{4.9}$$

Here, I, A and μ are the moment of inertia, area and the shear modulus, respectively, and l_0, l_1 and l_2 are the material parameters. Using the Hamilton's principle, we take the variation of the energies as

$$\delta\left[\int_{t_1}^{t_2}(T-U)\mathrm{d}t\right] = 0. \tag{4.10}$$

The corresponding expressions of δU and δT are [35]

$$\begin{aligned} \delta U = \int_0^L \Big[Sw^4 - Kw^6\Big]\delta w \mathrm{d}x + \Big[-Sw^3 + Kw^5\Big]\delta w\Big|_0^L \\ + \Big[Sw^2 - Kw^4\Big]\delta w'\Big|_0^L + Kw^3\delta w''\Big|_0^L \end{aligned} \tag{4.11}$$

and

$$\delta T = -\int_0^L \rho A\ddot{w}\delta w \mathrm{d}x. \tag{4.12}$$

Using Eqn. (4.11) and (4.12) in Eqn. (4.10), we obtain the governing equation of the beam under free vibration as

$$Sw^4 - Kw^6 + \rho A\ddot{w} = 0 \tag{4.13}$$

with following boundary conditions

$$\begin{aligned}
\big[V(L) - Sw^3(L) + Kw^5(L)\big]\delta w(L) - \big[V(0) - Sw^3(0) + Kw^5(0)\big]\delta w(0) = 0 \\
\big[M(L) + Sw^2(L) - Kw^4(L)\big]\delta w^{'}(L) - \big[M(0) + Sw^{''}(0) - Kw^4(0)\big]\delta w^{'}(0) = 0 \\
\big[M^h(L) + Kw^3(L)\big]\delta w^{''}(L) - \big[M^h(0) + Kw^3(0)\big]\delta w^{''}(0) = 0.
\end{aligned} \tag{4.14}$$

It is to be noted that when the two material parameters vanish, i.e., $l_0 = l_1 = 0$, then the governing equation reduces to that of modified couple stress theory as

$$(EI + \mu A l_2^2)w^4 + \rho A\ddot{w} = 0.$$

When all the material parameters vanish, i.e., $l_0 = l_1 = l_2 = 0$, then the governing equation reduces to that of classical theory as

$$(EI)w^4 + \rho A\ddot{w} = 0.$$

Approximating the deflection $w(x,t)$ as $w(x,t) = w_0(x)e^{\iota\omega t}$, the governing equation (4.13) reduces to the form

$$Sw_0^4 - Kw_0^6 - \rho A\omega^2 w_0 = 0. \tag{4.15}$$

Using the DQM, Eqn. (4.15) is re-written as

$$S\sum_{j=1}^{N} C_{ij}^4 w_j - K\sum_{j=1}^{N} C_{ij}^6 w_j - \rho A\omega^2 w_i = 0, \qquad i = 1, 2 \ldots N \tag{4.16}$$

4.2.2 Length scale parameter

As already pointed out in earlier sections that MCST comprises of an additional length scale parameter which captures the size effect. Similarly, MSGT consists of three additional length scale parameters to incorporate the size effect. Lam *et al* [77] proposed the higher order bending rigidity (b_h) as given by

$$b_h^2 = 6(1-2\nu)l_0^2 + \frac{2}{5}(4-\nu)l_1^2 + 3(1-\nu)l_2^2 \tag{4.17}$$

where, $l_0,\ l_1,\ l_2$ are the length scale parameters and ν is the Poisson's ratio. Additionally, Lam *et al* also experimentally determined the higher-order bending rigidity to be $b_h = 0.24\ \mu$m for $\nu = 0.38$. The length scale parameter l corresponding to MCST can be determined by putting $l_0 = l_1 = 0$ and

$l_2 = l$ in Eqn. (4.17) to obtain the relation

$$l = \sqrt{\frac{b_h^2}{3(1-\nu)}}. \tag{4.18}$$

Based on Eqn. (4.18), the value of length scale parameter is $l = 17.6$ μm [99, 106]. For determining the length scale parameters corresponding to MSGT, we use the assumption that $l_0 = l_l = l_2 = l_s$ [106]. Now, using the length scale parameters in Eqn. (4.17), we get

$$l_0 = l_1 = l_2 = l_s = \sqrt{\frac{b_h^2}{10.6 - 15.4\nu}}. \tag{4.19}$$

It gives the length scale parameter as $l_s = 11.01$ μm. Henceforth, we use these length scale parameters in our analysis.

4.3 Implementation of boundary conditions

For vibrational analysis of beams, there are two boundary conditions at the end $X = 0$ or $i = 1$ and another two at the other end $X = 1$ or $i = N$. As discussed earlier, we use the δ technique proposed by Bert *et al.* [79] and Jang *et al.* [97] for the clamped-free boundary conditions. This technique is simple and eliminates the difficulty of implementing two boundary conditions at one grid point. It applied one condition at each end at the boundary and the other at δ distance away. In other words, one boundary condition is applied at $X = 0$ and $X = \delta$ and the other condition at $X = 1 - \delta$ and $X = 1$. However, proper selection of δ is vital to ensure correct results [79]. In the δ technique, the boundary conditions are not correctly approximated as the conditions are not implemented exactly at the boundaries but at grid points adjacent to it. However, this technique works well for clamped-free end conditions but not for others. To do the vibrational analysis for beams with CC and SS end conditions we use another approach devised by Shu and Du [85] referred as SBCGE. The central idea of this technique is to implement all the four boundary conditions at the boundaries and not on adjacent grids. As a result, this technique is more accurate and works for all types of boundary conditions. In this technique, the boundary conditions are directly substituted into the governing equations. We use this technique for CC and SS beams.

4.3.1 Clamped-free beams

For cantilever beams with clamped-free end conditions, the boundary conditions given by Eqn. (4.14) are reduced to

$$w(0) = w^1(0) = 0, Kw^5(L) - Sw^3(L) = 0, Sw^2(L) - Kw^4(L) = 0. \tag{4.20}$$

The equivalent formulation in DQM at the clamped end $i = 1$ or $x = 0$ is

$$w_1 = 0, \qquad \sum_{j=1}^{N} C_{1j}^1 w_j = 0 \tag{4.21}$$

and that at the free end $i = N$ or $X = 1$ is

$$K\sum_{j=1}^{N} C_{Nj}^{5} w_j - S\sum_{j=1}^{N} C_{Nj}^{3} w_j = 0, \qquad S\sum_{j=1}^{N} C_{Nj}^{2} w_j - K\sum_{j=1}^{N} C_{Nj}^{4} w_j = 0. \tag{4.22}$$

Using the governing equation at the inner domain points and the boundary conditions at the end points, we write the equation in the matrix form as

$$[K][x] = \omega^2[M][x] \tag{4.23}$$

where, $[K]$ matrix is composed of

$$[K] = \begin{array}{c} i/j \\ 1 \\ 2 \\ 3 \\ \vdots \\ N-1 \\ N \end{array} \begin{array}{c} \begin{array}{ccccccccc} 1 & 2 & 3 & \cdots & \cdots & \cdots & \cdots & \cdots & N-1\,N \end{array} \\ \begin{bmatrix} [K_{bb1}] & [& & K_{bd1} & &] & [K_{bb2}] \\ [& & & & & &] & [&] \\ [& K_{db1} &] & [& K_{dd} &] & [& K_{db2} &] \\ [& &] & [& &] & [& &] \\ [K_{bb3}] & [& & K_{bd2} & &] & [K_{bb4}] \end{bmatrix} \end{array}$$

$$K_{bb} = \begin{bmatrix} K_{bb1} & K_{bb2} \\ K_{bb3} & K_{bb4} \end{bmatrix}$$

$$K_{bd} = \begin{bmatrix} K_{bd1} \\ K_{bd2} \end{bmatrix}$$

$$K_{db} = \begin{bmatrix} K_{db1} & K_{db2} \end{bmatrix}$$

.

A similar analogy also holds for $[M]$ matrix. Here, $[x] = [x_b \quad x_d]^T$, where, the subscripts $x_b = [X_1\ X_2\ X_{N-1}\ X_N]$ and $x_d = [X_3\ X_4\ \ldots\ X_{n-2}]$ represent boundary grid points and domain grid points, respectively. Re-writing Eqn. (4.23) in terms of boundary and domain points, we get

$$\begin{bmatrix} K_{bb} & K_{bd} \\ K_{db} & K_{dd} \end{bmatrix} \begin{bmatrix} x_b \\ x_d \end{bmatrix} = \omega^2 \begin{bmatrix} M_{bb} & M_{bd} \\ M_{db} & M_{dd} \end{bmatrix} \begin{bmatrix} x_b \\ x_d \end{bmatrix}. \tag{4.24}$$

For the boundary conditions, $[M_{bb}] = [M_{bd}] = [M_{db}] = [0]$. Re-arranging Eqn. (4.24) in the form of an eigen value problem, we get the final form of the equation as

$$[M_{dd}^{-1}\big(K_{dd} - K_{db}K_{bb}^{-1}K_{bd}\big)][x_d] = \omega^2[x_d]. \tag{4.25}$$

Equation (4.25) is then solved to obtain the natural frequencies ω.

4.3.2 Clamped-Clamped and simply supported beams

For CC and SS beams, the boundary conditions from Eqn. (4.14) are reduced to

$$w(0) = w^n(0) = 0, w(L) = w^n(L) = 0, \tag{4.26}$$

where, $n = 1$ corresponds to CC and $n = 2$ corresponds to SS beams. The equivalent formulation in DQM at the two clamped ends $i = 1$ or $X = 0$ is

$$w_1 = 0, \qquad \sum_{j=1}^{N} C_{1j}^{n} w_j = 0 \tag{4.27}$$

and that at the other clamped end $i = N$ or $X = 1$ is

$$w_N = 0, \quad \sum_{j=1}^{N} C_{Nj}^n w_j = 0. \tag{4.28}$$

These four boundary conditions cannot be applied at the two boundaries in the domain. Therefore, we apply the Dirichlet conditions at the ends. The derivative conditions are discretized using the DQ method. The discretized equations are then combined to determine w_2 and w_{N-1} which are back substituted into the governing equations applied to the interior (or domain) points. We follow the approach as given in Ref [85] and write the derivative boundary conditions for CC and SS beams in terms of w_2 and w_{N-1} as

$$\begin{aligned} w_2 &= \frac{1}{AXN} \sum_{j=3}^{N-2} AXK_1 w_j, \\ w_{N-1} &= \frac{1}{AXN} \sum_{j=3}^{N-2} AXK_N w_j, \end{aligned} \tag{4.29}$$

where,

$$\begin{aligned} AXK_1 &= C_{1,j}^n C_{N,N-1}^n - C_{1,N-1}^n C_{N,j}^n \\ AXK_N &= C_{1,2}^n C_{N,k}^n - C_{1,j}^n C_{N,2}^n \\ AXN &= C_{N,2}^n C_{1,N-1}^n - C_{1,2}^n C_{N,N-1}^n \end{aligned} \tag{4.30}$$

where $n = 1$ corresponds to CC case and $n = 2$ corresponds to SS case. Now, we substitute Eqn. (4.29) along with the Dirichlet boundary conditions of Eqn. (4.27) and (4.28) into the governing Eqn. (4.16) to obtain

$$\begin{aligned} S\Big(C_{i,2}^4 w_2 + \sum_{j=3}^{N-2} C_{i,j}^4 w_j + C_{i,N-1}^4 w_{N-1}\Big) - \\ K\Big(C_{i,2}^6 w_2 + \sum_{j=3}^{N-2} C_{i,j}^6 w_j + C_{i,N-1}^6 w_{n-1}\Big) - \rho A \omega^2 w_i = 0 \end{aligned} \tag{4.31}$$

After substituting Eqn. (4.29) into Eqn. (4.31), the governing equation is written in the form of Eqn. (4.23) corresponding to $N - 4$ grid points. The resulting equation reduces to an eigen value problem and is solved using available techniques.

4.4 Results and discussion

To do comparative study based on different theory, we take the beam dimensions and properties used in this paper as tabulated in Table 4.1. The natural frequencies for beams with different end conditions are obtained by solving the corresponding equations using the method as described in the previous sections. In order to present the robustness of DQM to solve vibrational problems, we first obtain the fundamental frequencies of beams with different end conditions corresponding

Table 4.1: The dimensions and the material properties used for the analysis.

Property	**Values**
Thickness	20 μm
Width	40 μm
Length	400 μm
E	1.44 GPa
μ	$\frac{0.5E}{(1+\nu)}$
ρ	1000 kgm^{-3}

Table 4.2: The first three non-dimensional frequencies for different types of beams. For simply supported and clamped-clamped beams, the SBCGE is used and for clamped-free beams, the δ technique is employed to determine the frequencies.

	Ω_1	Ω_2	Ω_3
simply supported			
Reference [85]	9.8696	39.4784	88.8264
Present	9.8689	39.4657	88.7957
clamped-clamped			
Reference [85]	22.3733	61.6728	120.9034
Present	22.3733	61.6726	120.9028
clamped-free			
Reference [68]	3.5160	22.0345	61.6972
Present	3.5199	22.0589	61.7657

to the classical theory by setting $l_0 = l_1 = l_2 = 0$ in our analysis. The non-dimensional frequency Ω obtained using the present method are then compared with results available in open literature. Table 4.2 presents the first three frequencies for different beams. We see that the results obtained using the present analysis agrees well with those available in literature. It is repeated here that the δ technique is used for beams with clamped-free end conditions while the SBCGE method is employed for analysis of other types of beams. It is to be noted that the SBCGE is a more correct method as it ensures that the boundary conditions are incorporated exactly at the boundaries, as a result this method always gives accurate results. The δ technique employs two boundary conditions at the boundary, and other two at δ distance away from the boundary. As a result although simpler, the δ technique does not give accurate results for all boundary conditions except clamped-free. For clamped-free end conditions, δ technique produces accurate results and is simpler in implementation.

Additionally, we also compare our results pertaining to the MCST. The present analysis can be reduced to that of MCST by setting the parameters $l_0 = l_1 = 0$. For the MCST, we compare our results of cantilever beams with that of Bekir and Omer [100] who used the RayleighRitz solution method to obtain the natural frequency for different material length scale parameters in Table 4.3. We see that our implementation is accurate and robust to handle beams with different types of end conditions for different theories. After validating our approach, we present the frequencies obtained using the MSGT.

Figures 4.1, 4.2 and 4.3 present the first three natural frequencies of microbeams with fixed-fixed, simply supported and fixed-free boundary conditions, respectively. For MCST $l_s = 17.6\mu$m and for MSGT $l_s = 11.01\mu$m are used with $\rho = 1200$ kgm^{-3} and $\nu = 0.38$. We see that the continuum theory underestimates the frequencies as it does not consider the size-dependent effects. When the

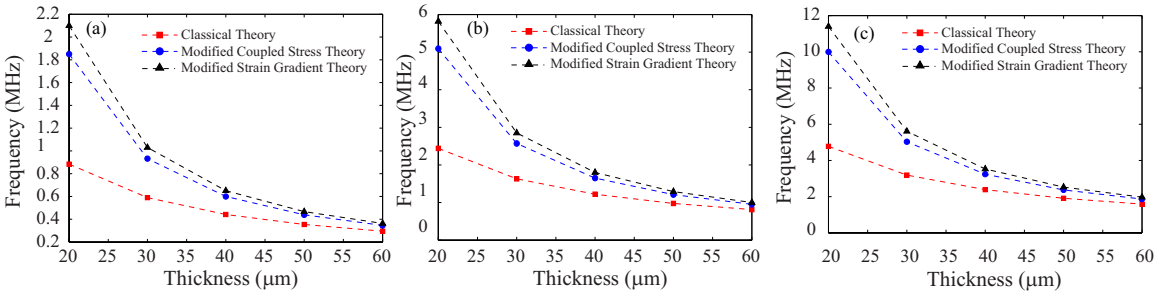

Figure 4.1: The first three natural frequencies of microbeams with fixed-fixed end conditions based on the continuum theory, the modified coupled stress theory ($l = 17.6\mu m$) and the modified strain gradient theory ($l_s = 11.01\mu m$).

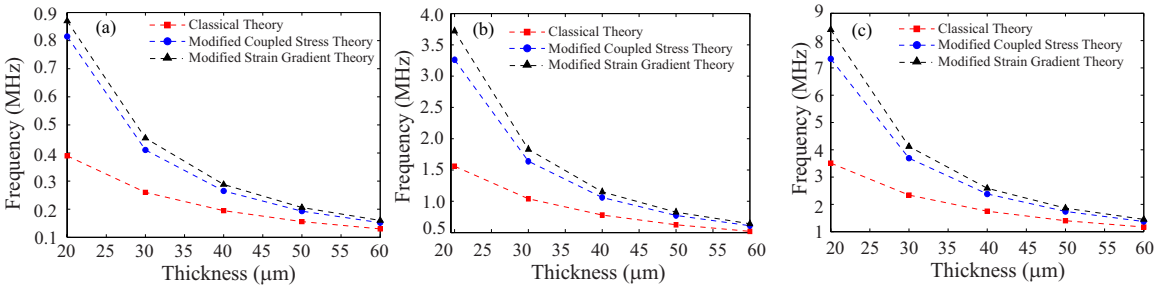

Figure 4.2: The first three natural frequencies of microbeams with simply supported end conditions on both ends based on the continuum theory, the modified coupled stress theory ($l = 17.6\mu m$) and the modified strain gradient theory ($l_s = 11.01\mu m$).

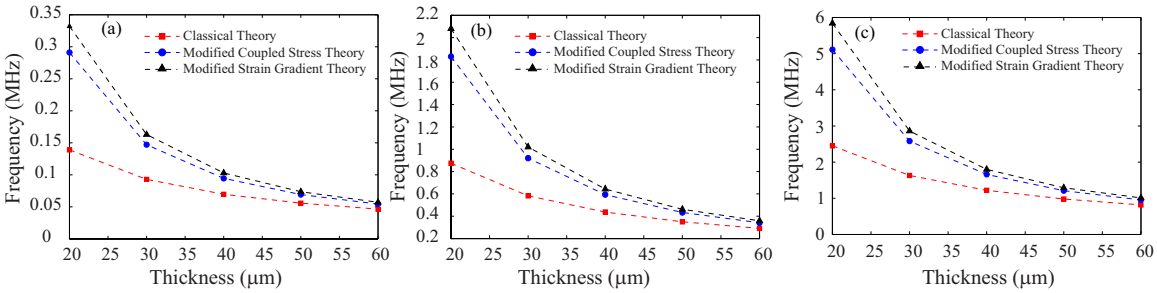

Figure 4.3: The first three natural frequencies of microbeams with fixed-free end conditions based on the continuum theory, the modified coupled stress theory ($l = 17.6\mu m$) and the modified strain gradient theory ($l_s = 11.01\mu m$).

Table 4.3: Comparison of first three frequencies for different material length scale parameters with the available results in literature.

	l=0.5h				l=h		
	Ω_1	Ω_2	Ω_3		Ω_1	Ω_2	Ω_3
Reference [100]	5.160	32.338	90.547		8.332	52.215	146.203
Present Method (DQM)	5.178	32.447	90.855		8.359	52.392	146.699

size effects are incorporated in the formulation, frequencies increase for all modes. It can be seen that the frequencies obtained by the MSGT is larger than that obtained using the MCST. It can also be noticed that when thickness of the beam is comparable to that of the length scale parameter, the difference in the frequencies obtained by the three theories is larger. As the thickness of the beam increases, the difference in frequencies continues to diminish. This is true irrespective of the end conditions and the modes of actuation. As a result, in order to obtain accurate results in MEMS and NEMS applications where the thickness of beams are usually of the order of few microns, it is very important to consider the size effects. Neglecting the size-effects undermines the frequencies as can be seen in Figs. 4.1-4.3.

4.5 Conclusions

In this paper, we have studied the dynamic characteristics of micro beams using the modified strain gradient elasticity theory. Additionally, we have also presented the behavior of beams employing the modified coupled stress theory. Beams with different end conditions like fixed-fixed, simply supported and fixed-free boundary conditions are analyzed. We have used the differential quadrature method which is fast accurate and robust method for studying the vibrational problems. It is found that the frequencies for all types of beams predicted by the modified strain gradient elasticity theory is larger than that predicted by the modified coupled stress theory which is in turn larger than the classical theory. However, as the thickness of the beam increases, the difference in frequencies obtained using the three methods continues to diminish. As a result, for application in micro/nano mechanics where size effects are appreciable, our analysis is vital to obtain correct frequencies for beams with different end conditions.

Chapter 5

Conclusions and future scope

The motive of the research presented in this thesis is to present the implementation of non-uniform beams for use as mechanical element in MEMS and NEMS devices and to study its effectiveness. At the same time, focus was laid to develop an analytical model for different aspects. In order to fulfill the aim of the thesis, following conclusions are drawn.

- In chapter 2, the nonlinear governing equation for a non-uniform beam is derived using Hamilton's principle. Henceforth, exact mode shapes is derived by transforming the beam equation for non-uniform beam to that of uniform beams. Subsequently, frequency equations is derived for different beams and are solved using Newton Ralphson to obtain the modal frequencies. At the same time, fundamental frequency under finite DC bias is obtained using Gelarkin's method and electrostatic softening is observed. It is also observed that the tuning could be done for a large frequency when non-uniform beams were used. Pull-in voltage is obtained using the dynamic equations and the variation of pull-in voltage with the non-uniformity parameter α is presented. It is concluded that employing non-uniform cantilever beams, specially converging beams with quartic variation in width corresponding to $\alpha = -0.6$ can exhibit improved performance both in terms of increased pull-in voltage as well as larger frequency tuning as compared to that of uniform beams.
- In chapter 3, the application of non-uniform beams in mass sensing is presented. The governing equation, mode shape and the boundary conditions obtained in Chapter 2 is modified to include the added tip mass effect. It is found that mass sensitivity increases significantly when non-uniform beams is used. At the same time, nonlinear dynamic study is also carried out to obtain the nonlinear frequency response of different types of non-uniform beams with tip mass. The method of multiple scales is used to obtain the modulation equations to plot the nonlinear frequency response. The influence of non-uniformity parameter α as well as tip mass μ on both linear frequencies as well as nonlinear frequency response is presented. It is found that the nondimensional sensitivity increases by a maximum factor of six when converging beams with quartic variation in width is employed. All converging beams have better sensitivity as compared to both uniform beams as well as diverging beams in which case sensitivity reduces drastically. It is also found that the nondimensional sensitivity further increases five folds when the beam is operated in its 5th mode. The analysis presented in Chapter 3, can prove to open a new dimension for fabricating high sensitivity mass sensors.

- In chapter 4, the effect of size related effects which becomes evident in low dimensional beams is analyzed. The conventional continuum theory (or local theory) fails to capture any size-effects as a result alternate non-local theories are used. The modified strain gradient elasticity theory (MSGT) which is a 6th order partial differential equation governing the equation of motion of beams is used to study the effect of size-effects on these beams. It is found that the dynamic characteristics specially the modal frequencies increases significantly when the size-effects are considered. Modal frequencies of beams with fixed-free, fixed-fixed and simply supported end conditions are plotted as a function of beam thickness. It is found that when the thickness of the beam is of the order of the material length scale parameter, significant changes occurs in the frequencies as compared to local theories. As the thickness increases, the difference in frequencies due to size-effects continues to diminish.

To sum up, the analytical model developed in this thesis can be used for designing and fabrication of MEMS devices with high performance. Additionally, use of non-uniform beams in MEMS based energy harvesters, array based sensors etc. can be explored in future.

Appendix A

Variation of kinetic and strain potential energy

The kinetic energy KE is given by

$$KE = \frac{1}{2}\int_0^l \rho A(x)\{\dot{u}^2 + \dot{w}^2\}dx.$$

Taking the variation of KE, we get

$$\delta KE = KE(\dot{u} + \delta\dot{u}, \dot{w} + \delta\dot{w}) - KE(\dot{u}, \dot{w}),$$

where,

$$KE(\dot{u} + \delta\dot{u}, \dot{w} + \delta\dot{w}) = KE(\dot{u}, \dot{w}) + \frac{\partial KE}{\partial \dot{u}}\delta\dot{u} + \frac{\partial KE}{\partial \dot{v}}\delta\dot{w}.$$

and, $\frac{\partial KE}{\partial \dot{u}} = \int_0^l \rho A(x)\dot{u}dx$ and $\frac{\partial KE}{\partial \dot{w}} = \int_0^l \rho A(x)\dot{w}dx$.
Integrating δKE from t_1 to t_2 and then simplifying the expression, we get

$$\int_{t_1}^{t_2} \delta KE = -\int_{t_1}^{t_2}\int_0^l \rho A(x)\ddot{u}\delta u dx - \int_{t_1}^{t_2}\int_0^l \rho A(x)\ddot{w}\delta w dx.$$

To find the variation of strain potential energy, the bending strain energy U_s can be written as

$$U_s = \frac{1}{2}\int_0^l EI(x)k^2 dx,$$

using k from Eqn. (2.2), U_s becomes

$$U_s = \frac{1}{2}\int_0^l EI(x)\bigg(\big(1 + \frac{\partial u}{\partial x}\big)\frac{\partial^2 w}{\partial x^2}\bigg)^2 + \bigg(\frac{\partial^2 u}{\partial x^2}\frac{\partial w}{\partial x}\bigg)^2 - 2\bigg(1 + \frac{\partial u}{\partial x}\bigg)\frac{\partial^2 w}{\partial x^2}\frac{\partial^2 u}{\partial x^2}\frac{\partial w}{\partial x}\}dx.$$

Taking the variation of U_s, we get

$$\delta U_s = U_s(u^{'} + \delta u^{'}, w^{'} + \delta w^{'}, u^{''} + \delta u^{''}, w^{''} + \delta w^{''}) - U_s(u^{'}, w^{'}, u^{''}, w^{''}),$$

where,

$$U_s(u^{'} + \delta u^{'}, w^{'} + \delta w^{'}, u^{''} + \delta u^{''}, w^{''} + \delta w^{''}) = U_s(u^{'}, w^{'}, u^{''}, w^{''}) + \frac{\partial U_s}{\partial u^{'}}\delta u^{'} + \frac{\partial U_s}{\partial w^{'}}\delta w^{'} + \frac{\partial U_s}{\partial u^{''}}\delta u^{''} + \frac{\partial U_s}{\partial w^{''}}\delta w^{''}$$

and,

$$\frac{\partial U_s}{\partial u^{'}} = \int_0^l EI(x)\bigg(\big(1 + \frac{\partial u}{\partial x}\big)\frac{\partial^2 w}{\partial x^2}\frac{\partial^2 w}{\partial x^2} - \frac{\partial^2 w}{\partial x^2}\frac{\partial^2 u}{\partial x^2}\frac{\partial w}{\partial x}\bigg)dx,$$

$$\frac{\partial U_s}{\partial w'} = \int_0^l EI(x)\left(\frac{\partial^2 u}{\partial x^2}\frac{\partial w}{\partial x}\frac{\partial^2 u}{\partial x^2} - \Big(1+\frac{\partial u}{\partial x}\Big)\frac{\partial^2 w}{\partial x^2}\frac{\partial^2 u}{\partial x^2}\right)dx,$$

$$\frac{\partial U_s}{\partial u''} = \int_0^l EI(x)\left(\frac{\partial^2 u}{\partial x^2}\frac{\partial w}{\partial x}\frac{\partial w}{\partial x} - \Big(1+\frac{\partial u}{\partial x}\Big)\frac{\partial^2 w}{\partial x^2}\frac{\partial w}{\partial x}\right)dx,$$

$$\frac{\partial U_s}{\partial w''} = \int_0^l EI(x)\left(\Big(1+\frac{\partial u}{\partial x}\Big)\frac{\partial^2 w}{\partial x^2}\Big(1+\frac{\partial u}{\partial x}\Big) - \Big(1+\frac{\partial u}{\partial x}\Big)\frac{\partial^2 u}{\partial x^2}\frac{\partial w}{\partial x}\right)dx.$$

Integrating δU_s from t_1 to t_2 and then simplifying it, we get

$$\begin{aligned}
\int_{t_1}^{t_2} -\delta U_s = &\int_{t_1}^{t_2}\int_0^l \left(EI(x)\Big(1+\frac{\partial u}{\partial x}\Big)\Big(\frac{\partial^2 w}{\partial x^2}\Big)^2\right)' \delta u dx - \int_{t_1}^{t_2}\int_0^l \left(EI(x)\frac{\partial^2 w}{\partial x^2}\frac{\partial^2 u}{\partial x^2}\frac{\partial w}{\partial x}\right)' \delta u dx \\
&+ \int_{t_1}^{t_2}\int_0^l \left(EI(x)\Big(\frac{\partial^2 u}{\partial x^2}\Big)^2\frac{\partial w}{\partial x}\right)' \delta w dx - \int_{t_1}^{t_2}\int_0^l \left(EI(x)\Big(1+\frac{\partial u}{\partial x}\Big)\frac{\partial^2 w}{\partial x^2}\frac{\partial^2 u}{\partial x^2}\right)' \delta w dx \\
&- \int_{t_1}^{t_2}\int_0^l \left(EI(x)\frac{\partial^2 u}{\partial x^2}\Big(\frac{\partial w}{\partial x}\Big)^2\right)'' \delta u dx + \int_{t_1}^{t_2}\int_0^l \left(EI(x)\Big(1+\frac{\partial u}{\partial x}\Big)\frac{\partial^2 w}{\partial x^2}\frac{\partial w}{\partial x}\right)'' \delta u dx \\
&- \int_{t_1}^{t_2}\int_0^l \left(EI(x)\Big(1+\frac{\partial u}{\partial x}\Big)^2\frac{\partial^2 w}{\partial x^2}\right)'' \delta w dx + \int_{t_1}^{t_2}\int_0^l \left(EI(x)\Big(1+\frac{\partial u}{\partial x}\Big)\frac{\partial^2 u}{\partial x^2})\frac{\partial w}{\partial x}\right)'' \delta w dx
\end{aligned}$$

Appendix B

Coefficient of the nonlinear governing equation

α	μ	S_1	S_2	S_3	S_4	S_5	α	μ	S_1	S_2	S_3	S_4	S_5
Linear variation in width													
0.1	0	11.66	36.87	5.68	5.68	0.063	-0.1	0	13.18	42.40	5.77	5.77	0.079
	0.05	9.84	24.16	5.80	5.80	0.058		0.05	10.82	25.36	5.91	5.91	0.072
	0.1	8.50	14.22	5.88	5.88	0.054		0.1	9.51	12.45	6.01	6.01	0.066
0.3	0.0	10.52	32.64	5.59	5.59	0.052	-0.3	0.0	15.34	49.88	5.84	5.84	0.103
	0.05	9.07	22.83	5.69	5.69	0.049		0.05	12.17	26.44	6.02	6.02	0.092
	0.1	7.97	14.95	5.76	5.76	0.045		0.1	10.10	9.55	6.14	6.14	0.084
0.6	0.0	9.25	27.93	5.47	5.47	0.041	-0.6	0.0	21.03	70.31	5.95	5.95	0.179
	0.05	8.17	20.85	5.54	5.54	0.039		0.05	17.52	43.48	6.14	6.14	0.163
	0.1	7.32	15.00	5.60	5.60	0.036		0.1	15.66	27.76	6.24	6.24	0.155
Quartic variation in width													
0.1	0.0	9.76	30.13	5.56	5.56	0.046	-0.1	0.0	15.96	52.69	5.90	5.90	0.111
	0.05	8.53	21.84	5.64	5.64	0.043		0.05	12.40	25.79	6.11	6.11	0.099
	0.1	7.56	15.07	5.70	5.70	0.040		0.1	10.12	6.58	6.25	6.25	0.089
0.3	0.0	6.38	18.57	5.27	5.27	0.021	-0.3	0.0	28.47	100.94	6.26	6.26	0.320
	0.05	5.90	15.63	5.31	5.31	0.020		0.05	17.23	-3.25	6.85	6.85	0.251
	0.1	5.50	13.03	5.34	5.34	0.019		0.1	12.27	-61.68	7.13	7.13	0.213
0.6	0.0	3.70	10.00	4.93	4.93	0.008	-0.6	0.0	85.28	319.26	6.42	6.42	2.365
	0.05	3.56	9.23	4.94	4.94	0.008		0.0025	74.19	210.53	6.84	6.84	2.26
	0.1	3.44	8.51	4.95	4.95	0.007		0.005	65.29	92.22	7.20	7.20	2.16
								0.01	52.23	-137.94	7.77	7.77	1.98

Table 1: Values of coefficients in modal dynamic equation given by Eqn. (3.9) for beams with varying mass ratio.

References

[1] A. K. Pandey, O. Gottlieb, O. Shtempluck, and E. Buks, Applied Physics Letter, 96, 203105 (2010).

[2] A. K. Pandey and R. Pratap, Journal of Micromechanics and Microengineering, 17(12), 2475 (2007).

[3] S. D. Vishwakarma, A. K. Pandey, J. M. Parpia, D. R. Southworth, H. G. Craighead, and R. Pratap, Journal of Microelectromechanical Systems, 23(2), 334-336 (2014).

[4] A. K. Pandey, Journal of Micromechanics and Microengineering, 23, 085015, (2013).

[5] P.N. Kambali, G. Swain, A. K. Pandey, E. Buks, O. Gottlieb, Applied Physics Letter, 104, 063104 (2015).

[6] A. K. Pandey, K.P. Venkatesh and R. Pratap, Sadhana, 34(4), 651-662 (2009).

[7] I. Kozinsky, H. W. Ch. Postma, I. Bargatin and M. L. Roukes, Applied Physics Letter, 88, 253101 (2006).

[8] P. N. Kambali and A. K. Pandey, Journal of Computational and Nonlinear Dynamics, 10(5), 051010 (2015)

[9] H. C. Nathanson, W. E. Newell, R. Wickstrom and J. R. Davis Jr, IEEE Transactions on Electron Devices, 14(3), 117-133 (1967)

[10] S. Pamidighantam, R. Puers, K. Baert and H. A. Tilmans, Journal of Micromechanics and Microengineering, 12(4), 458 (2002)

[11] P. M. Osterberg and S. D. Senturia, Journal of Microelectromechanical Systems, 6(2), 107-118 (1997)

[12] H. A. Tilmans and R. Legtenberg, Sensors and Actuators A: Physical, 45(1), 67-84 (1994)

[13] Y. Fang and P. Li, Journal of micromechanics and microengineering, 23(4), 045010 (2013)

[14] A. H. Nayfeh, M. I. Younis and E. M. Abdel-Rahman, Nonlinear dynamics, 41(1-3), 211-236 (2005)

[15] A. H. Nayfeh, M. I. Younis and E. M. Abdel-Rahman, Nonlinear dynamics, 48(1-2), 153-163 (2007)

[16] R. D. Blevins and R. Plunkett, Journal of Applied Mechanics, 47, 461 (1980)

[17] H. H. Mabie and C. B. Rogers, The Journal of the Acoustical Society of America, 55(5), 986-991 (1974)

[18] J. H.Lau, Journal of applied mechanics, 51(1), 179-181 (1984)

[19] H. H. Mabie and C. B. Rogers, The Journal of the Acoustical Society of America, 36(3), 463-469 (1964)

[20] F. W. Williams and J. R. Banerjee, Journal of Sound and Vibration, 99(1), 121-138 (1985)

[21] N. M. Auciello and G. Nole, Journal of Sound and Vibration, 214(1), 105-119 (1998)

[22] H.C. Wang, Journal of Applied Mechanics, 34(3), 702-708 (1967)

[23] C. Y. Wang, Archive of Applied Mechanics, 83(1), 171-176 (2013)

[24] S. Abrate, Journal of sound and vibration, 185(4), 703-716 (1995)

[25] S. Chowdhury, M. Ahmadi and W. C. Miller, Journal of Micromechanics and Microengineering, 15(4), 756 (2005)

[26] N. P. Van Der Meijs and J. T. Fokkema, Integration, the VLSI journal, 2(2), 85-119 (1984)

[27] K. Ramakrishnan and H. Srinivasan, Journal of Electrical Engineering,63(4), 242-248 (2012)

[28] S. Chaterjee and G. Pohit, Journal of sound and vibration, 322(4), 969-986 (2009)

[29] G. Li and N. R. Aluru, Sensors and Actuators A: Physical, 91(3), 278-291 (2001)

[30] M. Rasekh and S. E. Khadem, International Journal of Mechanical Sciences, 53(2), 108-115 (2011)

[31] M. Rahaeifard, M. H. Kahrobaiyan, M. Asghari and M. T. Ahmadian, Sensors and Actuators A: Physical, 171(2), 370-374 (2011)

[32] M. Baghani, International Journal of Engineering Science, 54, 99-105 (2012)

[33] J. Cheng, J. Zhe and X. Wu, Journal of Micromechanics and Microengineering, 14(1), 57 (2004)

[34] E. Lemaire, V. Rochus, J. C. Golinval, P. Duysinx, Computer Methods in Applied Mechanics and Engineering, 197(45), 4040-4050 (2008)

[35] M. Raulli, K. Maute, Structural and Multidisciplinary Optimization, 30(5), 342-359 (2005)

[36] M. M. Abdalla, C. K. Reddy, W. F. Faris and Z. Grdal, Computers and structures, 83(15), 1320-1329 (2005)

[37] F. Najar, S. Choura, E. M. Abdel-Rahman, S. El-Borgi and A. Nayfeh, Journal of micromechanics and microengineering, 16(11), 2449 (2006)

[38] F. Najar, S. Choura, S. El-Borgi, E. M. Abdel-Rahman and A. H. Nayfeh, Journal of Micromechanics and Microengineering, 15(3), 419 (2005)

[39] M. M. Joglekar and D. N. Pawaskar, Microsystem technologies, 17(1), 35-45 (2011)

[40] H. Shang-Rou, S. W. Shaw, and C. Pierre, Int. J. Solids Struct. **31**(14), 1981-2014 (1994)

[41] D. H. Hodges, AIAA J. **22**(12), 1825-1827 (1984)

[42] L. Meirovitch, Elements of vibration analysis. Vol. 2. New York: McGraw-Hill, (1986).

[43] Y. C. Hu, C. M. Chang, and S. C. Huang, Sensors and Actuators A: Physical, 112(1), 155-161 (2004)

[44] Ekinci, K. L., Huang, X. M. H., Roukes, M. L.:Ultrasensitive nanoelectromechanical mass detection. Applied Physics Letters. **84**, 4469-4471 (2004)

[45] Chaste, J., Eichler, A., Moser, J., Ceballos, G., Rurali, R., Bachtold, A.:A nanomechanical mass sensor with yoctogram resolution. Nature nanotechnology. **7**, 301-304 (2012)

[46] Fleming, W. J.:Overview of automotive sensors. Sensors Journal, IEEE, 1(4), 296-308 (2001)

[47] Van Beek, J. T. M., Puers, R.:A review of MEMS oscillators for frequency reference and timing applications. Journal of Micromechanics and Microengineering, 22(1), 013001 (2012)

[48] Kim, I. K., Lee, S. I.:Theoretical investigation of nonlinear resonances in a carbon nanotube cantilever with a tip-mass under electrostatic excitation. Journal of Applied Physics. 114, 104303 (2013)

[49] Kacem, N., Arcamone, J., Perez-Murano, F., Hentz, S.:Dynamic range enhancement of nonlinear nanomechanical resonant cantilevers for highly sensitive NEMS gas/mass sensor applications. Journal of Micromechanics and Microengineering, 20(4), 045023 (2010)

[50] Blevins, R. D., Plunkett, R.:Formulas for natural frequency and mode shape. Journal of Applied Mechanics. 47, 461 (1980)

[51] Ouakad, H. M., Younis, M. I.:Nonlinear dynamics of electrically actuated carbon nanotube resonators. Journal of Computational and Nonlinear Dynamics. 5, 011009 (2010)

[52] Mabie, H. H., Rogers, C. B.:Transverse vibrations of tapered cantilever beams with end loads. The Journal of the Acoustical Society of America. 36, 463-469 (1964)

[53] Mabie, H. H., Rogers, C. B.:Transverse vibrations of doubletapered cantilever beams with end support and with end mass. The Journal of the Acoustical Society of America. 55, 986-991 (1974)

[54] Lau, J. H.:Vibration frequencies of tapered bars with end mass. Journal of Applied Mechanics. 51, 179-181 (1984)

[55] Auciello, N. M., Nole, G.:Vibrations of a cantilever tapered beam with varying section properties and carrying a mass at the free end. Journal of Sound and Vibration. 214, 105-119 (1998)

[56] Wang, H.-C.:Generalized hypergeometric function solutions on transverse vibration of a class of nonuniform beams, Journal of Applied Mechanics, 34(3), 702-708 (1967)

[57] Williams, F. W., Banerjee, J. R.:Flexural vibration of axially loaded beams with linear or parabolic taper. Journal of Sound and Vibration. 99, 121-138 (1985)

[58] Wang, C. Y.:Vibration of a tapered cantilever of constant thickness and linearly tapered width. Archive of Applied Mechanics, 83, 171-176 (2013).

[59] Chaterjee, S., Pohit, G.:A large deflection model for the pull-in analysis of electrostatically actuated microcantilever beams. Journal of sound and vibration. 322, 969-986 (2009)

[60] Kambali, P. N., Pandey, A. K.:Nonlinear Response of a Microbeam Under Combined Direct and Fringing Field Excitation. Journal of Computational and Nonlinear Dynamics. 10, 051010 (2015)

[61] Caruntu, D. I., Martinez, I., Knecht, M. W.:Reduced order model analysis of frequency response of alternating current near half natural frequency electrostatically actuated MEMS cantilevers. Journal of Computational and Nonlinear Dynamics. 8, 031011 (2013)

[62] Abdel-Jaber, M. S., Al-Qaisia, A. A., Abdel-Jaber, M., Beale, R. G.:Nonlinear natural frequencies of an elastically restrained tapered beam. Journal of Sound and Vibration. 313, 772-783 (2008)

[63] Katsikadelis, J. T., Tsiatas, G. C.:Non-linear dynamic analysis of beams with variable stiffness. Journal of Sound and Vibration. 270, 847-863 (2004)

[64] Karimpour, S., Ganji, S. S., Barari, A., Ibsen, L. B., Domairry, G.:Nonlinear vibration of an elastically restrained tapered beam. Science China Physics, Mechanics and Astronomy. 55, 1925-1930 (2012)

[65] Clementi, F., Demeio, L., Mazzilli, C. E. N., Lenci, S.: Nonlinear vibrations of non-uniform beams by the MTS asymptotic expansion method. Continuum Mechanics and Thermodynamics. 27, 703-717 (2015)

[66] Singh SS, Pal P, Pandey AK. Pull-in analysis of non-uniform microcantilever beams under large deflection. Journal of Applied Physics.118(20):204303 (2015)

[67] Shang-Rou, H., Shaw, S. W., Pierre, C.:Normal modes for large amplitude vibration of a cantilever beam. International Journal of Solids and Structures. 31, 1981-2014 (1994)

[68] Hodges, D. H.:Proper definition of curvature in nonlinear beam kinematics. AIAA journal. 22, 1825-1827 (1984)

[69] Meirovitch, Leonard. Elements of vibration analysis. Vol. 2. New York: McGraw-Hill, (1986).

[70] Fleck NA, Muller GM, Ashby MF, Hutchinson JW. Strain gradient plasticity: theory and experiment. Acta Metallurgica et Materialia: 42(2):475-487 (1994)

[71] Stlken JS, Evans AG. A microbend test method for measuring the plasticity length scale. Acta Materialia :46(14):5109-5115 (1998)

[72] Lam DCC, Yang F, Chong ACM, Wang J, Tong P. Experiments and theory in strain gradient elasticity. Journal of the Mechanics and Physics of Solids:51(8): 1477-1508 (2003)

[73] Eringen AC, Edelen DGB. On nonlocal elasticity. International Journal of Engineering Science :10(3):233-248 (1972)

[74] Yang FA, Chong AC, Lam DC, Tong P. Couple stress based strain gradient theory for elasticity. International Journal of Solids and Structures. 39(10):2731-43 (2002)

[75] Lam DC, Yang F, Chong AC, Wang J, Tong P. Experiments and theory in strain gradient elasticity. Journal of the Mechanics and Physics of Solids.51(8):1477-508 (2003)

[76] Bellman R, Kashef BG, Casti J. Differential quadrature: a technique for the rapid solution of nonlinear partial differential equations. Journal of computational physics. 10(1):40-52 (1972)

[77] Bert CW, Jang SK, Striz AG. Two new approximate methods for analyzing free vibration of structural components. AIAA journal. 26(5):612-8 (1988)

[78] Bert CW, Xinwei W, Striz AG. Differential quadrature for static and free vibration analyses of anisotropic plates. International Journal of Solids and Structures. 30(13):1737-44 (1993)

[79] Bert CW, Wang X, Striz AG. Static and free vibrational analysis of beams and plates by differential quadrature method. Acta Mechanica. 102(1-4):11-24 (1994)

[80] Wang X, Bert CW. A new approach in applying differential quadrature to static and free vibrational analyses of beams and plates. Journal of Sound and Vibration 162(3):566-572 (1993)

[81] Wang X, Striz A, Bert CW. Free vibration analysis of annular plates by the DQ method. Journal of Sound and Vibration. 164(1):173-175 (1993)

[82] Wang X, Striz AG, Bert CW. Buckling and vibration analysis of skew plates by the differential quadrature method. AIAA journal. 32(4):886-9 (1994)

[83] Shu C, Du H. Implementation of clamped and simply supported boundary conditions in the GDQ free vibration analysis of beams and plates. International Journal of Solids and Structures. 34(7):819-35 (1997)

[84] Shu C, Generalized differential-integral quadrature and application to the simulation of incompressible viscous flows including parallel computation (Doctoral dissertation, University of Glasgow) (1991)

[85] Shu C, Richards BE. High resolution of natural convection in a square cavity by generalized differential quadrature. In Proceedings of the 3rd International Conference on Advances in Numeric Methods in Engineering: Theory and Application, Swansea, UK 978-985 (1990)

[86] Shu C, Richards BE. Application of generalized differential quadrature to solve twodimensional incompressible NavierStokes equations. International Journal for Numerical Methods in Fluids. 15(7):791-8 (1992)

[87] Shu C, Richard BE. Parallel simulation of incompressible viscous flows by generalized differential quadrature. Computing Systems in Engineering. 3(1):271-81 (1992)

[88] Tornabene F, Marzani A, Viola E, Elishakoff I. Critical flow speeds of pipes conveying fluid using the generalized differential quadrature method. Adv. Theor. Appl. Mech. 3(3):121-38 (2010)

[89] Reddy JN. Nonlocal theories for bending, buckling and vibration of beams. International Journal of Engineering Science. 45(2):288-307 (2007)

[90] Murmu T, Pradhan SC. Small-scale effect on the vibration of nonuniform nanocantilever based on nonlocal elasticity theory. Physica E: Low-dimensional Systems and Nanostructures. 41(8):1451-6 (2009)

[91] Janghorban M. Static analysis of tapered nanowires based on nonlocal Euler-Bernoulli beam theory via differential quadrature method. Latin American Journal of Solids and Structures. 9(2):1-0 (2012)

[92] Danesh M, Farajpour A, Mohammadi M. Axial vibration analysis of a tapered nanorod based on nonlocal elasticity theory and differential quadrature method. Mechanics Research Communications. 39(1):23-7 (2012)

[93] Chang TP. Small scale effect on axial vibration of non-uniform and non-homogeneous nanorods. Computational Materials Science. 54:23-7 (2012)

[94] imek M. Nonlocal effects in the free longitudinal vibration of axially functionally graded tapered nanorods. Computational Materials Science. 61:257-65 (2012)

[95] Jang SK, Bert CW, Striz AG. Application of differential quadrature to static analysis of structural components. International Journal for Numerical Methods in Engineering. 28(3):561-77 (1989)

[96] Al Kaisy AM, Esmaeel RA, Nassar MM. Application of the differential quadrature method to the longitudinal vibration of non-uniform rods. Engineering Mechanics. 14(5):303-10 (2007)

[97] Park SK, Gao XL. BernoulliEuler beam model based on a modified couple stress theory. Journal of Micromechanics and Microengineering. 16(11):2355 (2006)

[98] Akgz B, Civalek . Free vibration analysis of axially functionally graded tapered BernoulliEuler microbeams based on the modified couple stress theory. Composite Structures. 98:314-22 (2013)

[99] Ma HM, Gao XL, Reddy JN. A microstructure-dependent Timoshenko beam model based on a modified couple stress theory. Journal of the Mechanics and Physics of Solids. 56(12):3379-91 (2008)

[100] Salamat-talab M, Nateghi A, Torabi J. Static and dynamic analysis of third-order shear deformation FG micro beam based on modified couple stress theory. International Journal of Mechanical Sciences. 57(1):63-73 (2012)

[101] Chong CM. Experimental investigation and modeling of size effect in elasticity.2002

[102] Kong S, Zhou S, Nie Z, Wang K. The size-dependent natural frequency of BernoulliEuler micro-beams. International Journal of Engineering Science. 46(5):427-37 (2008)

[103] Akgz B, Civalek . Comment on Static and dynamic analysis of micro beams based on strain gradient elasticity theory by S. Kong, S. Zhou, Z. Nie, and K. Wang,(International Journal of Engineering Science, 47, 487498, 2009). International Journal of Engineering Science. 50(1):279-81 (2012)

[104] Dehrouyeh-Semnani AM. A comment on Static and dynamic analysis of micro beams based on strain gradient elasticity theory[Int. J. Eng. Sci. 47 (2009) 487498]. International Journal of Engineering Science. 90:86-9 (2015)